Version: 07.05.2021

Metal-ligand interface and internal structure of ultrasmall silver nanoparticles (2 nm)

Oliver Wetzel,[1] Shabnam Hosseini,[1] Kateryna Loza,[1] Marc Heggen,[2] Oleg Prymak,[1] Peter Bayer,[3] Christine Beuck,[3] Torsten Schaller,[4] Felix Niemeyer,[4] Claudia Weidenthaler,[5] and Matthias Epple[1]*

[1] Inorganic Chemistry and Center for Nanointegration Duisburg-Essen (CeNIDE), University of Duisburg-Essen, Universitaetsstr. 5-7, 45117 Essen, Germany

[2] Ernst Ruska-Centre for Microscopy and Spectroscopy with Electrons, Forschungszentrum Jülich GmbH, 52425 Jülich, Germany

[3] Department of Structural and Medicinal Biochemistry, Centre for Medical Biotechnology (ZMB), University of Duisburg-Essen, Essen, Germany

[4] Organic Chemistry, University of Duisburg-Essen, Universitaetsstr. 5-7, 45117 Essen, Germany

[5] Max-Planck-Institut für Kohlenforschung, Kaiser-Wilhelm-Platz 1, 45470 Mülheim an der Ruhr, Germany

* Corresponding author. e-mails: matthias.epple@uni-due.de

Abstract

Ultrasmall silver nanoparticles were prepared by reduction with $NaBH_4$ and surface-terminated with glutathione (GSH). The particles had a solid core diameter of 2 nm as shown by transmission electron microscopy (TEM) and small-angle X-ray scattering (SAXS). NMR-DOSY gave a hydrodynamic

diameter of 2 to 2.8 nm. X-ray photoelectron spectroscopy (XPS) showed that silver is bound to the thiol group of the central cysteine in glutathione under partial oxidation to silver(+I). In turn, the thiol group is deprotonated to thiolate. X-ray powder diffraction (XRD) together with Rietveld refinement confirmed a twinned (polycrystalline) fcc structure of ultrasmall silver nanoparticles with a lattice compression of about 0.9% compared to bulk silver metal. By NMR spectroscopy, the interaction between the glutathione ligand and the silver surface was analysed, also with ^{13}C-labelled glutathione. The adsorbed glutathione is fully intact and binds to the silver surface via cysteine. *In-situ* ^{1}H-NMR spectroscopy up to 85 °C in dispersion showed that the glutathione ligand did not detach from the surface of the silver nanoparticle, i.e. the silver-sulphur bond is remarkably strong. The ultrasmall nanoparticles had a higher cytotoxicity than bigger particles in *in vitro* cell culture with HeLa cells with a cytotoxic concentration of about 1 µg mL^{-1} after 24 h incubation. The overall stoichiometry of the nanoparticles was about $Ag_{\sim 250}GSH_{\sim 155}$.

Keywords: Silver; nanoparticles; NMR spectroscopy; glutathione; XPS spectroscopy

Introduction

There are many published results on gold nanoparticles, including their synthesis and physical, chemical, and biological properties. Usually, they are prepared by reduction of tetrachloroaurate with suitable reducing agents and surface-stabilized by the attachment of sulphur- or phosphorous-containing ligands. In classical syntheses, e.g. after Turkevich,[1] they have a diameter of about 15 nm and show a strong surface plasmon resonance. If a more strongly reducing agent like $NaBH_4$ is used (Brust-Schiffrin synthesis),[2-4] it is possible to prepare ultrasmall gold nanoparticles with a diameter of 1-2 nm. These are usually stabilized by thiol-

containing ligands which exploit the strong gold-sulphur bond.[5-9] The tripeptide glutathione (GSH) is one of the most common intracellular thiols.[10] It has also been used as stabilizing agent for ultrasmall gold nanoparticles and silver clusters.[11, 12]

Ultrasmall nanoparticles of silver have been studied to a much lesser extent than with gold, although a number of robust syntheses have been reported.[5, 7, 13-30] Ultrasmall gold-silver alloys have also been prepared.[31-33] Silver nanoparticles are well known for their interesting properties in heterogeneous catalysis,[34, 35] photonics,[36-38] biomedicine,[39, 40] and energy storage and conversion.[41] Silver is of particular interest due to its antibacterial action.[42] Together with the easy uptake of ultrasmall nanoparticles by cells, sometimes even into the nucleus,[43, 44] this is a promising pathway to combat bacteria. The biological effects of nanoparticles such as cell activation, cellular uptake and intercellular distribution are all affected by size, shape, structure and surface charge of the nanoparticles.[45-50] Smaller silver particles may release silver ions faster, causing a higher antibacterial effect due to an increased local silver ion concentration.[51, 52]

Silver is less noble than gold, and the silver-sulphur bond is considered as weaker than the gold-sulphur bond,[53] although the binding situation in metal clusters is generally complex.[54, 55] It is therefore of interest to shed more light on the metal-ligand interface which is possible by NMR spectroscopy and X-ray photoelectron spectroscopy (XPS). Furthermore, the ultrasmall particle size might also affect the interaction between the silver atoms in the metallic core, leading to a change in the lattice parameters compared to microcrystalline silver. Here we present the results of a comprehensive study of the core as well as of the surface structure of glutathione-coated ultrasmall silver nanoparticles.

Experimental

Chemicals

For the synthesis of silver nanoparticles, we used silver nitrate ($AgNO_3$, Carl Roth, 99%) and sodium borohydride ($NaBH_4$, Fluka, 96%). The particles were coated either with L-glutathione (GSH, Sigma Aldrich, 98%) or with isotope-labelled glutathione, Glu-C*(^{13}C3,^{15}N)-Gly, which was obtained from Caslo (purity 95.6% by HPLC, 99% degree of labelling for both ^{13}C and ^{15}N). The Ag-GSH nanoparticles were fluorescently labelled with NHS-fluorescein (5/6-carboxyfluorescein succinimidyl ester, Thermo Fisher Scientific, >90%).

Ultrapure water with a specific resistivity of 18.2 MΩ was prepared with a Purelab ultra instrument (ELGA) and used for all experiments unless noted otherwise. All glassware was cleaned with boiling aqua regia and washed thoroughly with ultrapure water.

Nanoparticle synthesis

In a typical synthesis, 6.8 mg $AgNO_3$ (40 µmol) and 36.8 mg GSH (120 µmol) was dissolved in 20 mL degassed water and stirred vigorously for 30 min. Then 15 mg $NaBH_4$ (400 µmol, freshly dissolved in 1 mL cold water) was added and the mixture was stirred for another 30 min. The dark-red Ag-GSH nanoparticle dispersion was purified by centrifugation through an ultrafiltration spin column (MWCO 3 kDa, 15 mL; Amicon; Merck) for 45 min at 4,000 rpm (2,500 g). The purified nanoparticles were freeze-dried (lyophilized) with a Christ Alpha 2-4 LSCplus instrument and stored at 4 °C until further application. A typical yield of such a synthesis was 10 mg. The nanoparticles were easily redispersible in water by gentle shaking.

For fluorescent labelling of the GSH on the surface of the silver nanoparticles (only for cell culture studies), 4.3 mg (9.1 µmol) of NHS-fluorescein was dissolved in 100 µL dimethylformamide and added to 10 mL borate buffer (pH 8.5) containing 100 µg (Ag content) of the silver particles and reacted at 8 °C for

12 h. The purification was done by centrifugation through an ultrafiltration spin column until no fluorescein was detectable in the filtrate (UV spectroscopy).

Cell uptake studies

Cell studies with GSH-coated ultrasmall silver nanoparticles were carried out with human cervix carcinoma cells (HeLa).[56] The cells were cultured in Dulbecco's modified Eagle's medium (DMEM), supplemented with 10% fetal bovine serum (FBS, Gibco), 100 U mL^{-1} penicillin, and 100 U mL^{-1} streptomycin at 37 °C in humidified atmosphere with 5% CO_2. To assess the cytotoxicity of the silver nanoparticles, the cells were trypsinized and seeded in a 24-well culture dish with $2.5 \cdot 10^4$ cells per well in 500 µL cell culture medium to the experiments. After 24 h cell cultivation, different amounts of the water-dispersed silver nanoparticles were added to the cells. The cytotoxicity of the nanoparticles was determined with a 3-(4,5-dimethylthiazol-2-yl)-2,5-diphenyltetrazolium bromide (MTT) cytotoxicity assay. For this, the cells were washed three times with 500 µL PBS and incubated with 300 µL MTT solution (1 g L^{-1}) for 1 h at 37 °C. Then the MTT solution was replaced by 300 µL DMSO, and the cells were incubated for 30 min. Finally, sample triplicates of DMSO were transferred to a 96-well plate (100 µL aliquots) for spectrophotometric analysis with a Multiskan FC instrument (Thermo Fisher Scientific Inc., Waltham, MA, USA) at 570 nm. The relative cell viability was calculated in comparison to a control group of untreated cells.

To analyse the uptake of nanoparticles by HeLa cells, the cells were trypsinised and seeded in a glass bottom dish with 10^4 cells per well in 250 µL cell culture medium 24 h prior to the experiments. The cells were then incubated for 24 h with 250 µL of different concentrations of fluorescein-labelled silver nanoparticles. The cells were then washed three times with 300 µL PBS. After the completed incubation, the cells were fixed with 100 µL 4% aqueous formaldehyde for 20 min at room temperature and washed again three times with 300 µL PBS each.

Prior to actin staining, the cells were permeabilized with 150 µL 0.1% Triton X-100 for 5 min and washed twice with 300 µL PBS each. For actin staining, the cells were incubated with 150 µL of a solution of 25 µg mL^{-1} Alexa Fluor® 660-phalloidin (Invitrogen, Karlsruhe, Germany) in PBS with 1% bovine serum albumin and then washed three times with 150 µL PBS each. The cell nucleus was stained with 150 µL of a 10 µg mL^{-1} solution of Hoechst33342 (Life Technologies, Eugene, OR, USA) for 15 min. The cells were washed three times with 300 µL PBS each, stored in 250 µL PBS, and finally analysed with a Leica TCS SP8 confocal laser scanning microscope with a 63X water objective.

Analytical methods

The silver concentration in the nanoparticle dispersion was determined by atomic absorption spectroscopy (AAS) with a Thermo Electron M-Series spectrometer (graphite tube furnace; procedure according to DIN EN ISO/IEC 17025:2005) after dissolving the nanoparticles in *aqua regia*. Elemental analysis (C, H, N, S) was carried out with a Euro Vector EURO EA Elemental Analyzer according to DIN EN ISO/IEC 17025:2005.

Analytical disc centrifugation (differential centrifugal sedimentation; DCS) was performed with a CPS Instruments DC 24000 disc centrifuge (24,000 rpm). Two sucrose solutions (8 wt% and 24 wt%) formed a density gradient that was capped with 0.5 mL dodecane as stabilizing agent. The calibration standard was a poly(vinyl chloride) (PVC) latex in water with a particle size of 483 nm provided by CPS Instruments. A calibration was carried out prior to each run. A sample volume of 100 µL of dispersed nanoparticles was used. The measuring time was about 10 h at the given centrifugation speed due to the small particle size. The density of elemental silver (10,490 kg m^{-3}) was used for the computations.

UV-VIS spectroscopy was performed with a Varian Cary 300 instrument from 200 to 800 nm after background solvent correction (PBS buffer). Suprasil® quartz glass cuvettes with a sample volume of 500 µL were used.

High-resolution transmission electron microscopy was performed with an aberration-corrected FEI Titan transmission electron microscope equipped with a Cs-probe corrector (CEOS Company) operating at 300 kV.[57]

For NMR spectroscopy, up to 10 mg of the GSH-coated silver nanoparticles were dispersed in 500 µL D_2O. All silver nanoparticle dispersions were prepared in D_2O (pH 8.3). 1D-NMR spectra (^1H, ^{13}C) and 2D-NMR spectra (^1H-^1H-COSY, ^1H-^{13}C-HSQC, ^1H-^{13}C-HMBC) were recorded with an Avance III 600 MHz spectrometer (Bruker, Rheinstetten, Germany) equipped with a Prodigy cryo probe head. Temperature-dependent ^1H-NMR experiments were performed on a Bruker DRX 500 MHz instrument. Due to the low ligand concentration in the aqueous dispersions, all ^1H-NMR spectra were recorded with simultaneous suppression of the water signal by excitation sculpting; the excited spectral range had a width of approximately 0.6 ppm. The number of GSH molecules on the particle surface was determined by quantitative ^1H-NMR spectroscopy with maleic acid as external standard and the ERETIC routine.[58]

DOSY-NMR spectroscopy was performed with a Bruker Avance III 700 MHz spectrometer with a 5 mm TCI $^1H/^{13}C/^{15}N$/D cryoprobe with a *z*-gradient in a 3-mm sample tube at 25 °C. The ^1H-DOSY pulse sequence from the Bruker library was modified with a pre-saturation pulse to suppress the remaining water signal. For the DOSY experiments, the diffusion time Δ was 100 ms, and the pulsed gradient duration δ was 2 ms for free glutathione and 3.5 ms for GSH-coated nanoparticles. For each pseudo-2D DOSY data set, the gradient strength was incrementally increased from 5 to 95% of the maximum gradient strength (50.4 G cm^{-1} for a smoothed square gradient pulse) in 32 steps with a linear ramp.

^{1}H,^{13}C-iDOSY-HSQC measurements at the natural abundance of ^{13}C (unlabelled GSH) were recorded with a constant time delay (including the diffusion period) of 56 ms, a diffusion gradient pulse length of 1.5 ms, with 176 scans and 128 increments in the indirect dimension. The gradient strength was incrementally increased from 5 to 95% of the maximum in 11 steps with a linear ramp.

The spectra were Fourier-transformed, phased, and integrated with the program Topspin 3.5 (Bruker). The linearized diffusion data were plotted and fitted according to the Stejskal-Tanner equation[59, 60]

$$\ln\left(\frac{I}{I_0}\right) = -\gamma^2 \delta^2 \left(\Delta - \delta/3\right) \cdot D \cdot G^2 \qquad (1)$$

with I the signal intensity, I_0 the signal intensity without gradient, γ the gyromagnetic ratio of ^{1}H, δ the diffusion gradient pulse length, Δ the diffusion delay, G the gradient strength, and D the translational diffusion coefficient.

The Stejskal-Tanner plots of four well-discernible proton signals of free glutathione (3.7 ppm, 3.0 ppm, 2.55 ppm, 2.15 ppm) and five signals of GSH-coated silver nanoparticles (3.8 ppm, 3.4 ppm, 3.2 ppm, 2.6 ppm, 2.2 ppm) were first analysed separately. Upon yielding the same diffusion coefficient within the error margin, the relative intensities I/I_0 of all signals were averaged. Error bars of the averaged data points represent the standard deviation of these three proton signals. The given accuracy of the diffusion coefficient is the standard deviation of the Stejskal-Tanner fit.

The hydrodynamic diameter was calculated according to the Stokes-Einstein equation

$$d_H = \frac{k_B \cdot T}{3\pi \cdot \eta \cdot D} \qquad (2)$$

with d_H the hydrodynamic diameter, k_B the Boltzmann constant, T the temperature in K, η the dynamic viscosity of D_2O at 25 °C,[61] and D the translational diffusion coefficient.

X-ray photoelectron spectroscopy (XPS) was performed with a spectrometer from SPECS GmbH equipped with a Phoibos 150 1D-DLD hemispherical energy analyser. The monochromatised Al Kα X-ray source (E=1486.6 eV) was operated at 15 kV and 200 W. For high-resolution scans, the pass energy was set to 20 eV. The medium area mode was used as lens mode. The base pressure in the analysis chamber was $5 \cdot 10^{-10}$ mbar during the experiment. To account for charging effects, all spectra were referred to C 1s at 284.5 eV.

X-ray powder diffraction (XRD) was performed on a D8 Advance diffractometer (Bruker) in reflection mode with Cu Kα radiation (λ=1.54 Å; U=40 kV, I=40 mA, line focus). A dispersion of GSH-coated silver nanoparticles was mixed with microcrystalline LaB_6 standard powder from NIST (SRM 660b) and placed on a silicon single crystal sample holder to minimize scattering. After drying in air, the sample was measured from 20 to 90° 2Θ with a step size of 0.01° and a counting time of 12 s, resulting in a total measurement time of 24 h. Qualitative phase analysis was performed with Diffrac.Suite EVA V1.2 from Bruker with the patterns of cubic Ag (#4-0783)[62] and LaB_6 (#34-0427)[63] from the ICDD database. Quantitative Rietveld refinement was performed with the Bruker software TOPAS 5.0 to calculate the lattice parameters a and the average crystallite size CS from diffraction peak broadening.[64, 65] The reference material LaB_6 was necessary for instrumental parameter correction and the precise determination of the sample displacement as refined in the Rietveld procedure.

Small-angle X-ray scattering (SAXS) was performed on an Empyrean diffractometer (Panalytical) in transmission mode with evacuated beam path ScatterX-78, Cu Kα radiation (λ=1.54 Å, U=40 kV and I=40 mA, line focus) and a sample-to-detector distance of 240 mm. As incident beam optics, a focusing X-

ray mirror and a 1/32° SAXS divergence slit with an opening of 0.05 mm were used. A PIXcel^{3D} detector with a mounted shielding device suppressed undesirable scattering in scanning line detector mode (1D). For 1D-SAXS measurements, a glass capillary (length 80 mm, outer diameter 1 mm, wall thickness 0.01 mm) was filled with a colloidal dispersion of GSH-coated silver nanoparticles in water. For background correction, the same capillary was filled with water and measured again. The capillary was measured in the ScatterX-78 device at a vacuum of $1.4 \cdot 10^{-2}$ mbar in the 2Θ range of -0.15° to 5.00° at a step size 0.01° with a total measurement time of 21 min.

For the SAXS modelling, a polydisperse system of spheres was considered using an indirect Fourier transformation (IFT) procedure based on the algorithms implemented in GNOM module.[66] The SAXS analysis was done with the EasySAXS software 2.0 from Panalytical which enables a determination of the volume-weighed size distribution (DV) from the measured scattering intensity $I(q)$ with the form factor of the spheres $P_{sph}(q,R)$. The overall equation for the scattering intensity[67] was

$$I(q) = c_v \int_0^\infty D_v(R) \cdot R^3 \cdot P_{sph}(q,R) \cdot dR \tag{3}$$

with c_v a constant, q the reciprocal space momentum transfer modulus, defined as $q=4\ \pi\ \sin(\Theta)/\lambda$, R the radius of the spheres, $D_v(R)$ the size distribution function weighted by volume, and $P_{sph}(q,R)$ the form factor for the spheres, which is defined as

$$P_{sph}(q,R) = F^2{}_{sph}(q) = \left[3\frac{\sin(qR) - qR\cos(qR)}{(qR)^3} \right]^2 \tag{4}$$

The original SAXS data were deconvoluted to take into account the linear beam focus of the ScatterX[78] stage in the diffractometer.

The SAXS curve represents a q-region up to q_{max} = 0.35 Å^{-1} comprising the Guinier region (up to q_{Gui} = 0.21 Å^{-1}) and the middle region (q_{mid} = 0.21 to 0.35 Å^{-1}). With the radius R of 0.8 nm from the average size of the spherical particles, the Guinier radius of gyration[68] can be calculated as $R_G = \sqrt{(3/5)}\cdot R \approx 0.62$ nm. Using the Guinier law (valid when $q_{min}\cdot R_G < 1.3$ Å^{-1}),[69] one obtains $q_{Gui} \sim 0.2$ Å^{-1}. Since our SAXS data goes up to q_{max}=0.35 Å^{-1}, this is a reasonable estimation of the particle size from the recorded SAXS curve.

Results and discussion

The ultrasmall silver nanoparticles had a mostly spherical shape in HRTEM, including a twinned crystal structure (Figure 1).

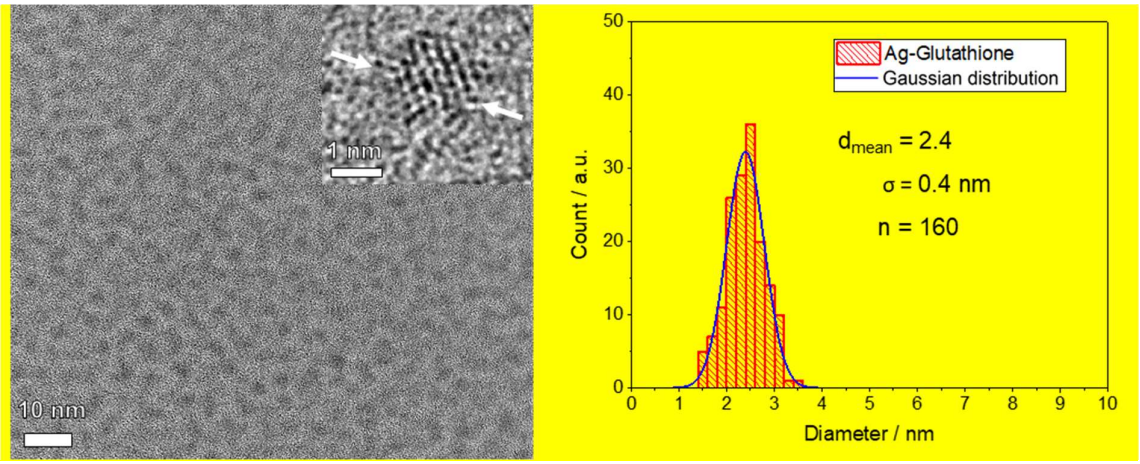

Figure 1: HRTEM image of GSH-coated silver nanoparticles with particle size distribution analysis. The inset shows an atomic resolution image of one nanoparticle where the twin boundary is indicated by white arrows.

Disc centrifugal sedimentation gave an average particle diameter of 1.9 nm (Figure 2). However, it is known that DCS systematically underestimates the

particle size because the effective density of an ultrasmall nanoparticle is lower than that of the pure metal due to the presence of the ligand shell.[70] UV spectroscopy confirmed the absence of larger particles as the surface plasmon resonance typical for silver nanoparticles (380 to 420 nm)[71] was not observed (Figure 2). The particles were not autofluorescent due to their small size as shown by fluorescence spectroscopy (data not shown).[6, 72]

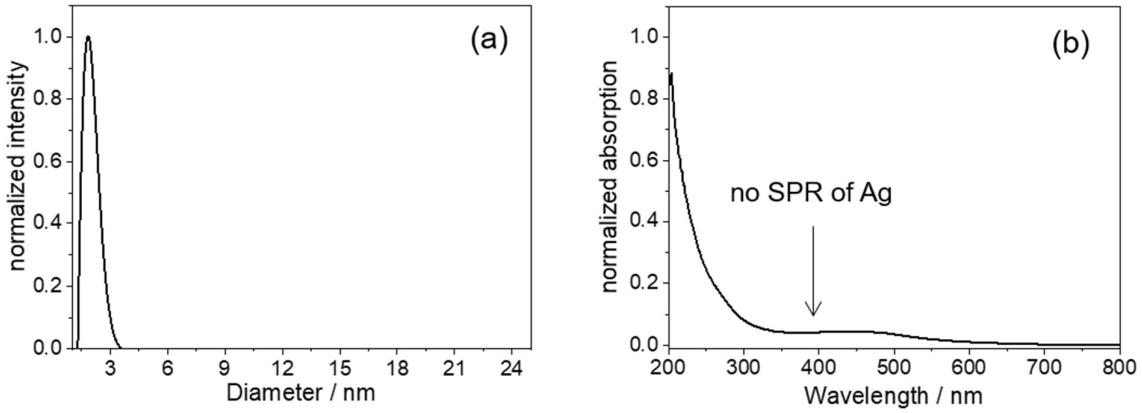

Figure 2: Particle size distribution of GSH-coated silver nanoparticles determined by disc centrifugal sedimentation (DCS; **a**), and optical properties determined by UV/VIS spectroscopy (**b**).

X-ray powder diffraction showed very broad diffraction peaks of nanocrystalline silver and sharp peaks of the added microcrystalline LaB_6 (Figure 3). This indicated that the sample did not contain larger particles which would have given rise to sharp diffraction peaks. It also did not contain any contaminations from other potential crystalline compounds like salts from the synthesis. Rietveld refinement showed that GSH-coated ultrasmall silver nanoparticles had a significantly compressed unit cell (a=4.05±0.01 Å) compared to microcrystalline Ag (a=4.087±0.001 Å; ICDD #4-0783).[62, 73, 74] This lattice compression of about 0.9% agrees with the literature.[75] The calculated crystallite size (CS=0.9±0.1 nm) was smaller than the particle size (2 nm by TEM), indicating a polycrystalline

(twinned) structure of the nanoparticles in accordance with earlier results on ultrasmall gold nanoparticles,[76] general crystallographic considerations on small nanoparticles,[77] and our TEM analysis given in Figure 1. The XRD results further demonstrate that the ultrasmall nanoparticles prepared here still have the fcc structure of the bulk silver metal (albeit twinned), unlike atom-sharp clusters.[5, 19, 55, 78-88] However, the presence of single-crystalline particles cannot be ruled out, therefore it is possible that the sample contains both single-crystalline and twinned particles. Furthermore, the low number of atoms in each particle causes surface defects and contributes to X-ray diffraction peak broadening as well. Extensive HRTEM studies would be required to determine the fractions of each particle type.

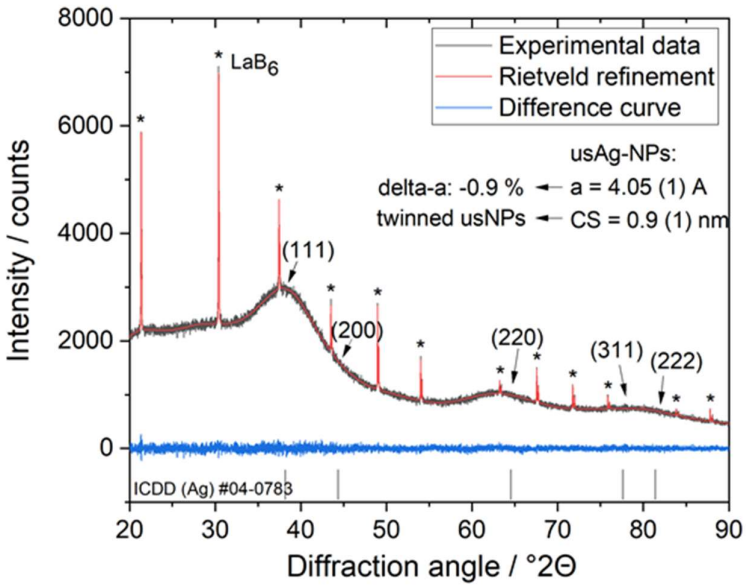

Figure 3: Representative X-ray powder diffractogram with qualitative phase analysis and Rietveld refinement (R_{wp}=2.7) of GSH-coated silver nanoparticles (usAg-NPs) mixed with LaB_6 (peak splitting due to Cu $K\alpha_{1,2}$ radiation at higher diffraction angles). The asterisks indicate the narrow diffraction peaks of the reference compound LaB_6. The numbers in parentheses indicate the Miller indices of the broad diffraction peaks of silver.

Small-angle X-ray scattering (SAXS) of dispersed nanoparticles showed a monomodal size distribution, a good colloidal dispersion, and a diameter of the metal core of 1.6 nm (Figure 4; see also Materials and Methods).[89, 90] The particle size is in a good agreement with the results by TEM and DCS. Note that the given particle size distribution by SAXS is based on the counting of a much larger number of nanoparticles (order of millions) compared to TEM (order of hundreds). This explains the differences in the particle sizes from SAXS (1.6 nm) and TEM (2.0 nm). However, the values are close enough to indicate a good agreement between the two methods. If we assume an average diameter of the

metallic core of 2 nm and a spherical shape, each particle consists of about 250 silver atoms.[91]

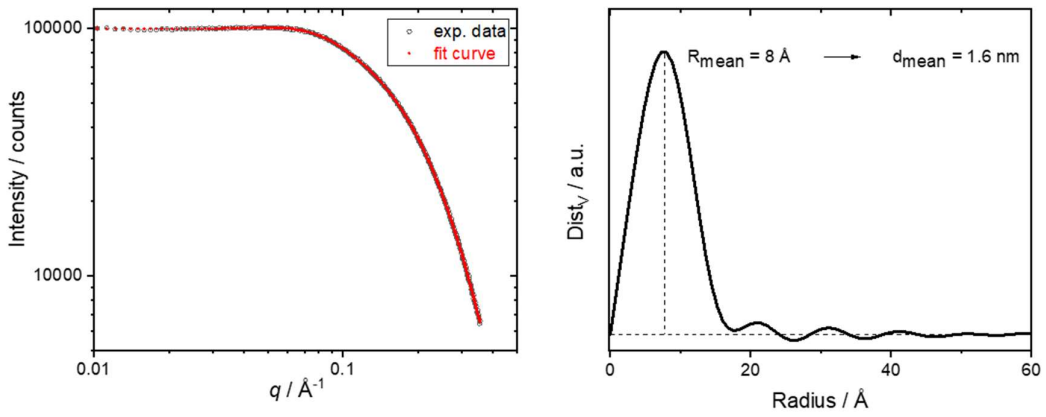

Figure 4: Results of small-angle X-ray scattering (SAXS) of dispersed GSH-coated silver nanoparticles with experimental data and model fit (**left**) and volume-weighed size distribution $Dist_v$ (**right**). The average particle size (metal core) was 1.6 nm.

Due to the small size of the nanoparticles, it is possible to perform NMR spectroscopy on dispersed ultrasmall particles.[11, 92-96] Only the ligand shell can be observed as the metallic core is not susceptible to NMR.[97] ^{1}H-DOSY NMR spectroscopy (Figure 5) gave the hydrodynamic diameter of the dispersed particles (including the ligand shell) of 2.8±0.1 nm, while ^{1}H,^{13}C-iDOSY-HSQC gave a diameter of 2.05±0.10 nm.

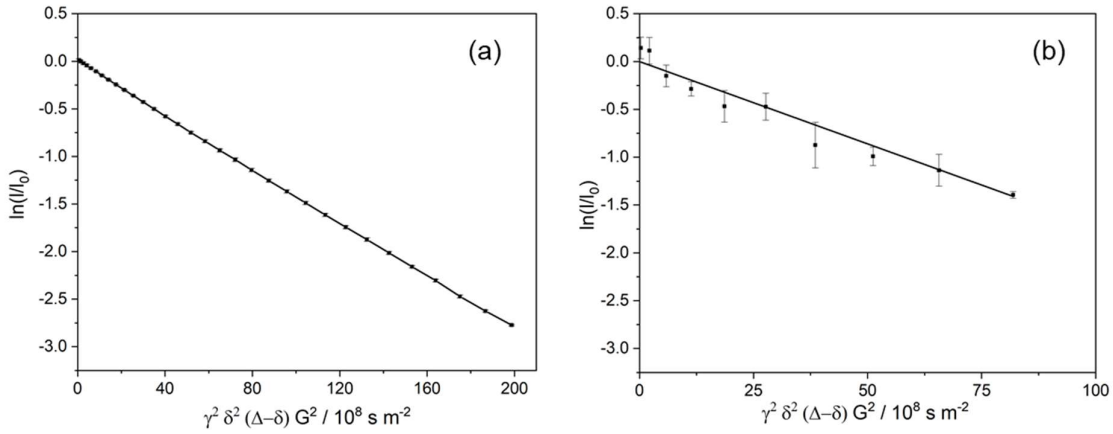

Figure 5: Stejskal-Tanner plot of ^{1}H-DOSY (**a**) and ^{1}H,^{13}C-iDOSY-HSQC (**b**) NMR data of GSH-coated silver nanoparticles. Data points are the average of all analysed ^{1}H signals and the error bars represent the standard deviation of the mean. The negative slope equals the translational diffusion coefficient.

Based on an average core diameter of 2 nm, elemental analysis (C, H, N, S, Ag) of the nanoparticles gave 160 GSH molecules per silver nanoparticle, which is in good agreement with the results of quantitative ^{1}H-NMR spectroscopy (see below) where approximately 150 GSH molecules per nanoparticle were found. The molecular footprint was 0.08 nm^2 per GSH molecule. This is in good agreement with earlier studies on ligand-coated ultrasmall gold nanoparticles (Table 1). Note that the metallic radii of gold and silver are almost identical and that both crystallize in an fcc lattice. For a 2 nm particle, a stoichiometry of $Ag_{\sim 250}GSH_{\sim 155}$ can be derived. With molecular weights of 107.87 g mol^{-1} (Ag) and 307.32 g mol^{-1} (GSH), this corresponds to a molecular mass per nanoparticle of about 74.6 kDa with 36 wt% Ag and 64 wt% GSH.

Table 1: Literature data on ligand footprints on ultrasmall silver and gold nanoparticles. OAA: Cysteine-containing oligo(amidoamine)s.[98] Tweezers: Molecular tweezers[99]. AA: Amino acids.

Particle type	Nanoparticle core diameter / nm	Number of ligands per nanoparticle	Ligand footprint on the surface / nm^2
GSH-coated silver nanoparticles (this work)	2	150 to 160	0.08
Cysteine-coated gold nanoparticles[94]	1.78	$Au_{\sim 174}$(cysteine)$_{\sim 67}$	0.15
Azide-terminated gold nanoparticles (Au-N_3)[93]	2	117 azide and 117 lysine	0.053 each
FAM-clicked gold nanoparticles[44, 93]	2	7 to 9	1.48
Cy3-clicked gold nanoparticles [44]	2	4-6	2.5
Tweezer-clicked gold nanoparticles[100]	2	11 to 30	0.42 to 1.14
Peptide (6 to 9 AA)-coated gold nanoparticles[76]	2	ca. 150	0.084
CRaf peptide (36 AA)-coated gold nanoparticles[101]	1.55	16-20	0.41
OAA-coated gold nanoparticles[92]	2	36 to 99	0.15 to 0.40 per OAA; 0.06 to 0.1 per cysteine

The chemical nature of the interface between sulphur-containing ligands and noble metal nanoparticles is usually described as covalent M-S bond, sometimes including metal complexes on the surface of a metallic core.[53, 55, 102-104] To elucidate the chemical environment of the binding atoms, XPS was applied. For the identification of the oxidation state and the chemical environment of Ag in the

silver nanoparticles, the reference compounds Ag_2S, AgI, and AgBr were analysed (Figure 6). The Ag 3d high-resolution spectrum of the GSH-functionalized nanoparticles (Ag $3d_{5/2}$ 368.1 eV) matched well with the photopeaks obtained for Ag_2S (Ag $3d_{5/2}$ 368.0 eV). In contrast, the peak maxima of the other reference materials were significantly shifted to higher (AgI, Ag $3d_{5/2}$ 368.4 eV) or lower (AgBr, Ag $3d_{5/2}$ 367.7 eV) binding energies. The assignment of the binding energy of the Ag $3d_{5/2}$ photopeak to the oxidation state of silver requires the consideration of the position of the Auger peak as well as the presence or absence of energy loss lines because the core level shifts are not very sensitive to the oxidation state of silver. The accepted value of the Ag $3d_{5/2}$ photopeak of Ag^0 is 368.3 eV, and the Auger parameter is 726.5 eV.[105] Although the photopeak at 368.1 eV measured for the coated silver nanoparticles is close to the literature values of Ag_2S, the binding energy value can also be assigned to metallic Ag. However, the Auger parameter of the coated nanoparticles of 723.8 eV is much closer to the literature value of Ag_2S (724.8 eV)[106] than to that of metallic Ag (726.5 eV).[105] Another important spectral feature of metallic Ag are energy loss lines at 372 and 378 eV which were not observed for the GSH-coated silver nanoparticles. The analysis of the Ag 3d spectrum therefore indicates that Ag is fully in the oxidation state Ag^+ with a chemical environment similar to that of Ag_2S, AgCl, or Ag_2O.

If we take the number of about 250 silver atoms per particle, about 50% of the silver atoms are present on the particle surface. The fact that we have a clear indication for an oxidation state of Ag(+I) suggests that the "metallic Ag(0) atoms" inside the particle are also experiencing a partial oxidation by the bound thiolate groups. Clearly, there is no strict electronic separation between "oxidized silver atoms" on the surface and "metallic silver atoms" inside the particle.

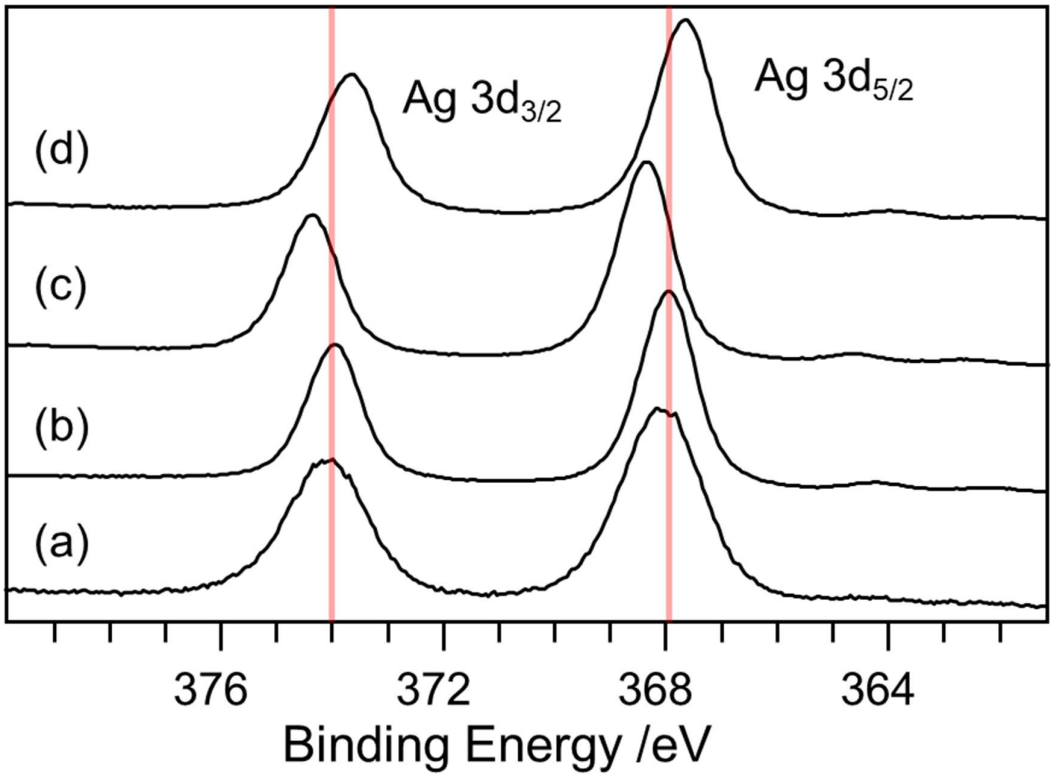

Figure 6: Ag 3d high resolution photo peaks of GSH-coated ultrasmall silver nanoparticles (**a**) and the three reference compounds: Ag_2S (**b**), AgI (**c**), and AgBr (**d**). The red vertical lines indicate the peak shifts of the silver nanoparticles compared to the reference materials.

A further evaluation of the high-resolution S 2p spectra can help to assign the observed sulphur species to specific bonds (Figure 7). Sulphur atoms chemically bound to metal atoms of nanoparticles show peaks between ~161 and 162.5 eV.[107-109] The S 2p spectrum of pure glutathione contained the doublets S $2p_{3/2}$ (163.3 eV) and S $2p_{1/2}$ (164.5 eV) that are characteristic for organic sulphur in thiol groups.[110] For sulphur on the silver nanoparticles, the S $2p_{3/2}$ peak was shifted to 162.0 eV (S $2p_{1/2}$ 163.1 eV). The shift of the sulphur peak to lower binding energies (S $2p_{3/2}$162.0 eV) was also observed for glutathione on a gold surface which indicates a negative charge of the sulphur binding to gold, i.e. the presence

of thiolate.[111] High-resolution XPS spectra were also measured for the main ligand elements carbon, nitrogen and oxygen (Figure S1)

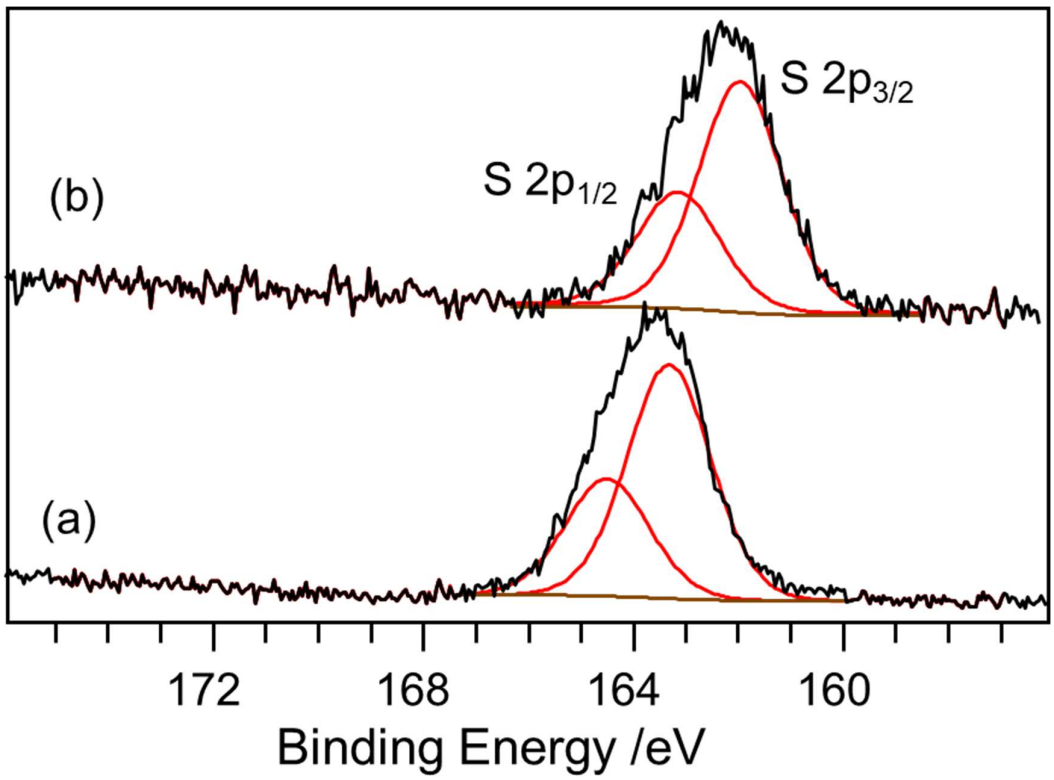

Figure 7: XPS high-resolution spectra of the S 2p photoelectrons of glutathione (GSH) (**a**) and of GSH-coated silver nanoparticles (**b**).

In Figure 8, the ^{1}H-NMR spectra of GSH and of dispersed GSH-coated silver nanoparticles are displayed. In aqueous dispersion, the ^{1}H resonances of GSH showed a rather moderate pH-sensitivity: Only the signal of H1 was significantly shifted. At pH 8.3, the spectrum of particle-bound GSH resembled that of dissolved GSH, but the NMR peaks were considerably broadened. In addition, the two diastereomeric β-protons (denoted as H3) were less shielded, resulting in a downfield shift whereas the chemical shifts of all other protons were less affected by the vicinity to the silver nanoparticle. Nevertheless, the peaks were still well

separated and could be unambiguously assigned to the individual protons by the ^{1}H COSY spectrum (Figure 9).

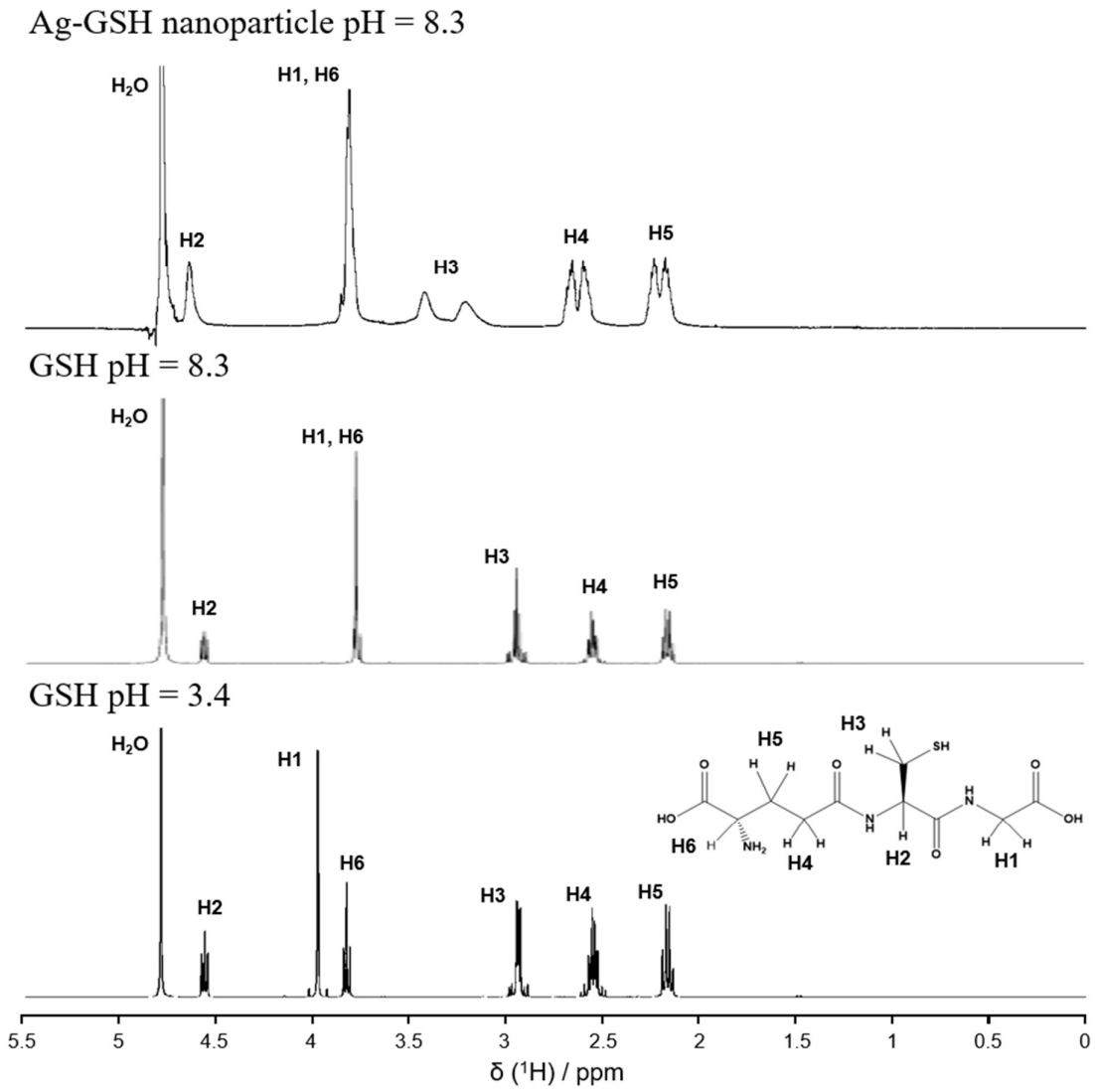

Figure 8: ^{1}H-NMR spectra of dissolved glutathione at pH 3.4 and 8.3, respectively, and of glutathione-coated silver nanoparticles at pH 8.3. For the proton assignment see also Figure 9.

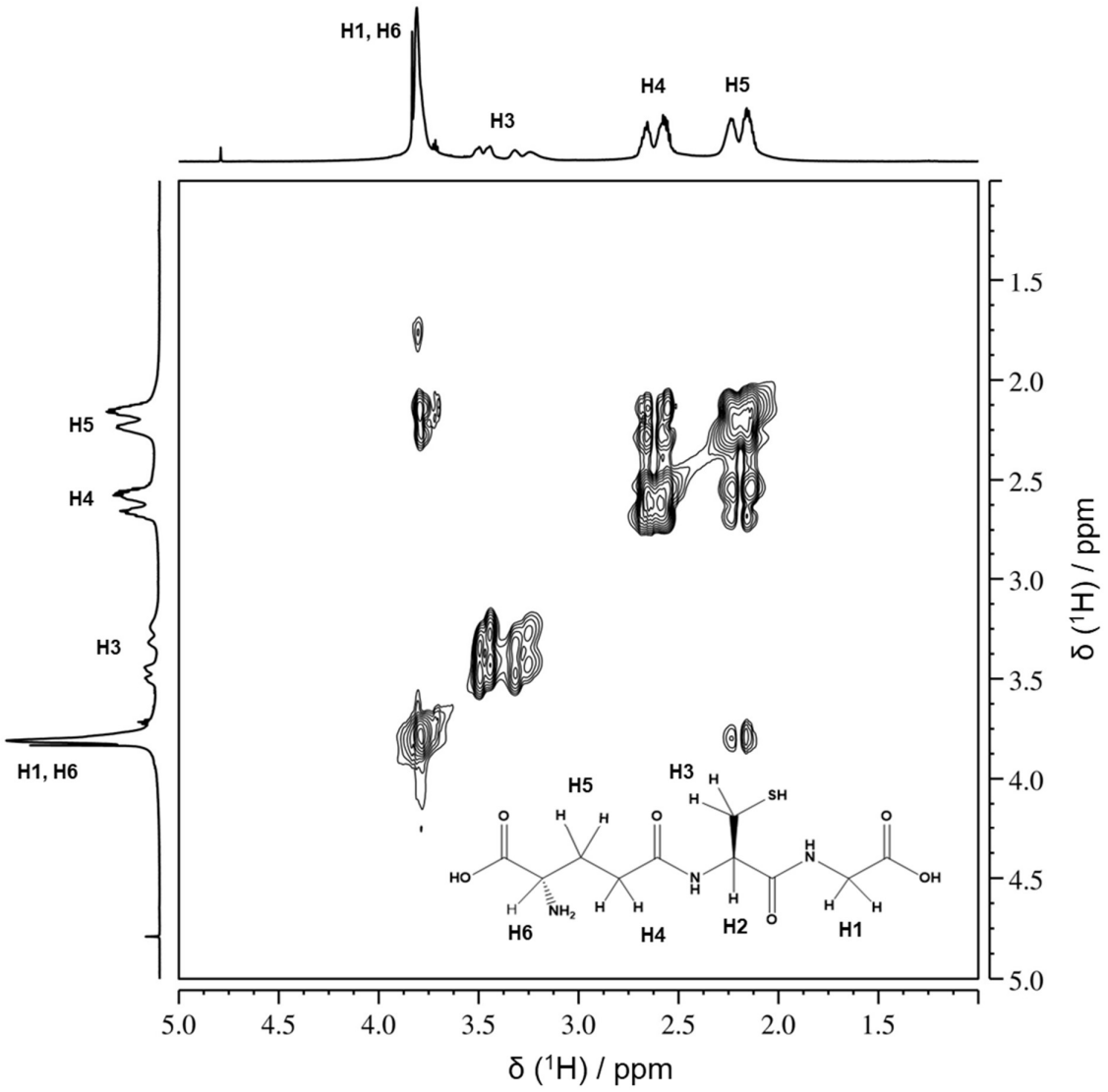

Figure 9: ^{1}H-^{1}H-COSY NMR spectrum of GSH-coated silver nanoparticles. Note that the spectrum was recorded with suppression of the water signal by excitation sculpting, resulting in the loss of the H2 signal at 4.55 ppm.

The observation of line broadenings and simultaneous shift of signals assigned to protons in close proximity to the metal surface is in good agreement with earlier reports on NMR spectroscopy of ultrasmall gold nanoparticles[11, 92-96] and other investigations focusing on small molecules on the surface of nanoparticles.[112, 113] Notably, the ^{1}H-NMR spectrum recorded here is very similar to that recorded for

GSH on gold nanoparticles.[11] There, the authors had assigned the line broadening of all signals to a distribution of different chemical environments.

This interpretation was supported by ^{13}C-NMR spectroscopy (Figure 10). In comparison with the spectrum of dissolved GSH, all signals of the GSH-coated silver nanoparticles were broadened; the signal of C3, i.e. the carbon atom which is closest to the silver surface, was hardly observable. Again, the peaks of the cysteine carbon atoms, C3 and C2 were shifted downfield by 10.2 and 2.4 ppm, respectively.

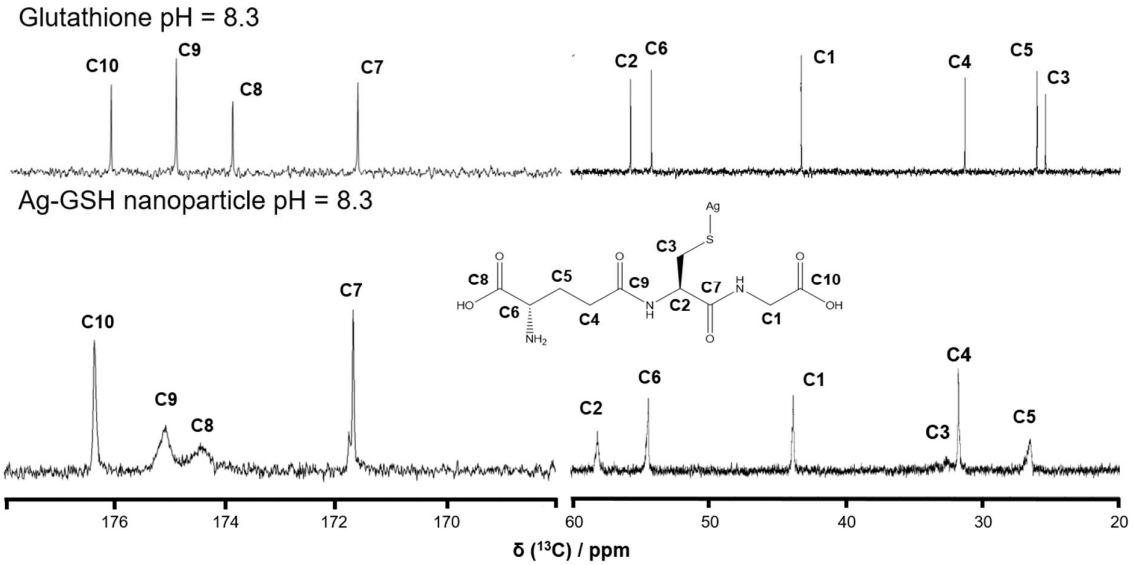

Figure 10: ^{13}C-NMR spectra of dissolved GSH and glutathione-coated ultrasmall silver nanoparticles at pH 8.3.

An unambiguous assignment of all ^{1}H and ^{13}C peaks of GSH was achieved by ^{1}H-^{13}C-HSQC and HMBC NMR experiments probing the bonds between protons and carbon atoms. HMBC was necessary to assign the signals of the carbonyl carbon atoms. Most importantly, the observation of all expected correlation peaks indicates that the GSH was still fully intact after the conjugation to the silver surface.

A close inspection of the ^{1}H-^{13}C-HSQC spectrum (Figure 11) showed additional signals for the β-CH_2 group of cysteine (C3, H3). Besides the intense correlation peak (33.3 ppm/3.5 and 3.3 ppm), a second set of ^{1}H signals, even broader and shifted downfield by 0.07 ppm, was observed. The corresponding ^{13}C signal, identified by its small, but distinct correlation peak at 32.6 ppm could not be detected in the conventional ^{13}C-NMR spectrum due to its low intensity and large line width. This CH_2 group is obviously most sensitive due to the vicinity of the metal surface; therefore, it is a good probe to elucidate the structural specifics of GSH-silver interaction. The HMBC experiment in Figure 12 showed the carbonyl carbon signals and thereby permitted the assignment of all carbon signals.

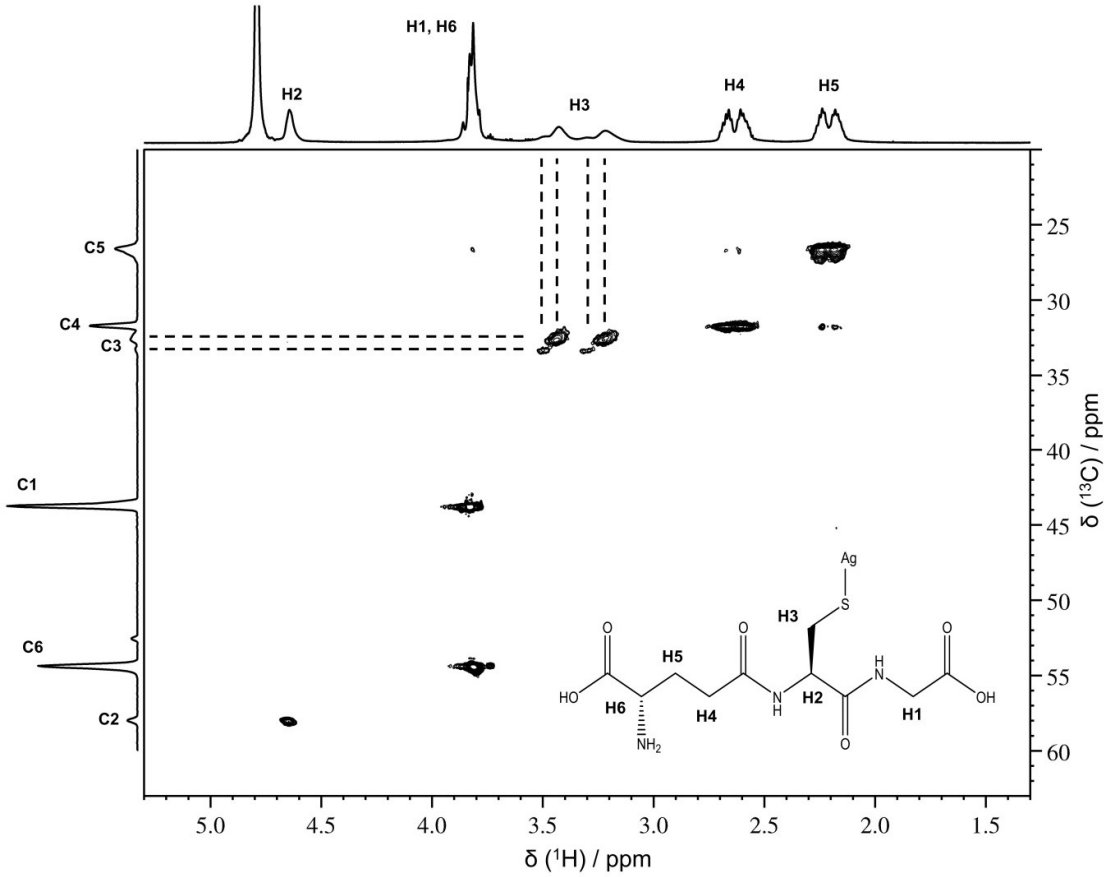

Figure 11: The ^{1}H-^{13}C-HSQC NMR spectrum of GSH-coated silver nanoparticles shows correlations between covalently bound carbon and hydrogen atoms.

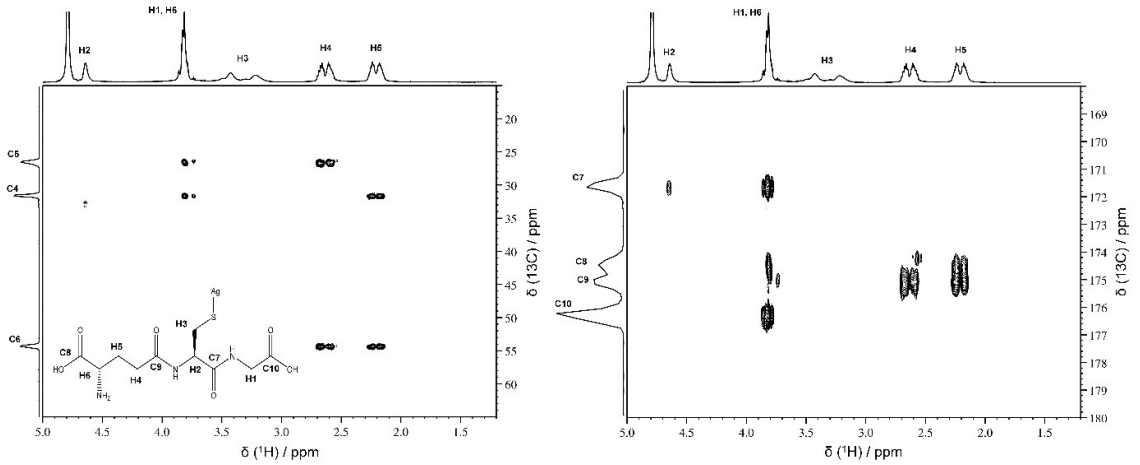

Figure 12: ^{1}H-^{13}C-HMBC NMR spectrum of GSH-coated silver nanoparticles. Aliphatic region (**left**) and correlation of the CH-protons to the carbonyl groups (**right**).

By ^{1}H-NMR spectroscopy, we quantified the number of GSH molecules on the silver nanoparticle. For this purpose, an aqueous solution of maleic acid of known concentration was measured as external standard. The ^{1}H-NMR spectrum of dispersed GSH-coated silver nanoparticles (without suppression of the water signal to avoid intensity glitches) was then subjected to the ERETIC routine,[58] giving the concentration of GSH molecules in the dispersion. The number of nanoparticles was determined by measuring the silver concentration and assuming a 2 nm diameter of each particle. We found that approximately 155 GSH molecules were bound to the surface of each nanoparticle, in good agreement with the results from elemental analysis.

A way to gain a deeper insight into the binding situation is the use of isotope-labelled ligands to enhance the NMR sensitivity for non-hydrogen atoms. In our previous study, a ^{13}C enrichment provided information on the binding sites of cysteine on the surface of an ultrasmall gold nanoparticle.[94] Here, we used ^{13}C-labeled cysteine as part of GSH (Figure 13). The characteristic splitting due to ^{13}C-^{13}C homonuclear coupling together with their chemical shift indicates the

presence of residual GSH-disulphide (GSSG) molecules not bound to the silver surface. The two signals at 38.7 ppm and 52.9 ppm correspond to C3 and C2 of the GSSG molecule. The GSSG was already detected as impurity in the ^{13}C-labelled glutathione and apparently accumulated during synthesis and purification of the particles. Again, the peaks assigned to GSH bound to the nanoparticle were significantly broadened with the linewidth of the C2-signal being smaller than that of C3. Nevertheless, the C3-resonance appeared to consist of two components with slightly different chemical shifts in agreement with the observation from the ^{1}H-^{13}C-HSQC spectrum: A deconvolution of the rather noisy C3-peak gave chemical shifts of 33.2 and 32.5 ppm for two constituting peaks. This indicates the occurrence of at least two distinct β-CH_2 moieties experiencing different magnetic environments on the particle surface.

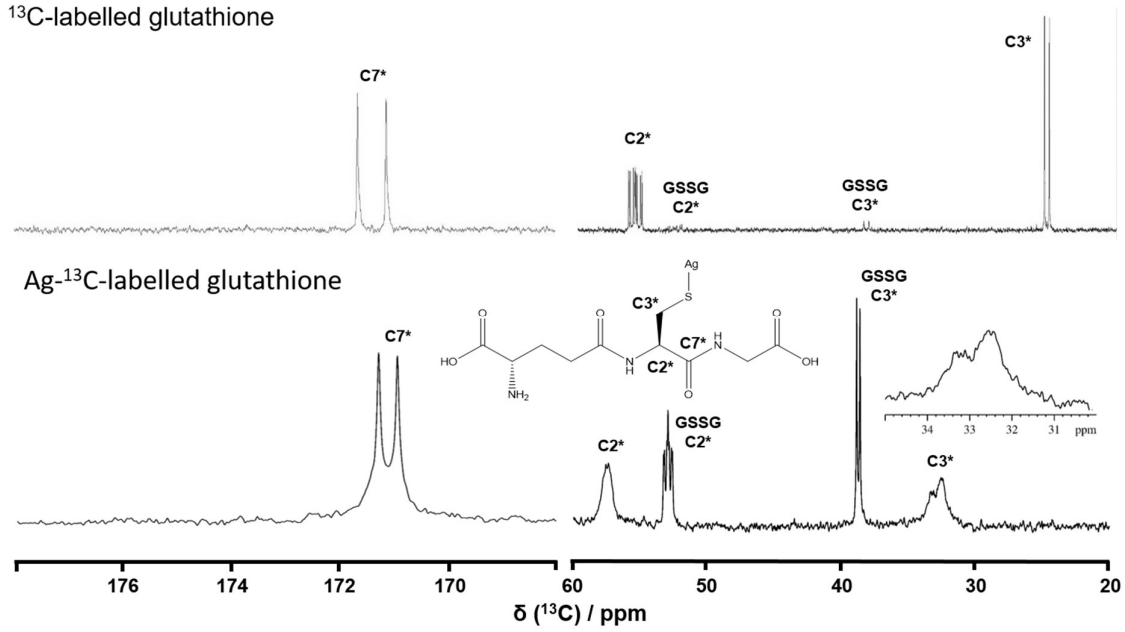

Figure 13: ^{13}C-NMR spectra of cysteine-labelled GSH and GSH-coated Ag nanoparticles.

Glutathione has been shown to replace polyacrylic acid and to disintegrate 6.4 nm silver nanoparticles to 1.3 nm silver nanoparticles, demonstrating its strong binding to the silver surface.[20] On the other hand, glutathione is rapidly replaced by 4-fluorothiophenol, demonstrating the different stability of Au-S bonds.[114] To elucidate the thermal stability of the particle-ligand bond, we recorded ^{1}H-NMR spectra at enhanced temperatures up to 85 °C (Figure 14). The spectra of the dispersed nanoparticles showed neither a temperature-dependent shift nor a significant change in the spectrum. The spectrum remained the same after cooling, indicating that the ligand shell remained fully intact and was not affected by the heating procedure. Moreover, dissociated ligand molecules were not observed which would have been clearly identified by their narrow peak widths. The signals for H2 and H3, however, showed some peculiarities. The H2 signal, usually not detectable in a ^{1}H-NMR experiment due to the overlapping suppression of the water signal, was observed above 65 °C due to the temperature-dependent shift of the water resonance (suppressed). The most remarkable change was observed for the signals assigned to the H3 methylene protons which displayed complex changes in their line shapes. A conclusive interpretation of the observed changes is far from trivial; however, it is clear that the spectral features cannot be explained by only one β-CH_2 moiety in cysteine (C3/H3).

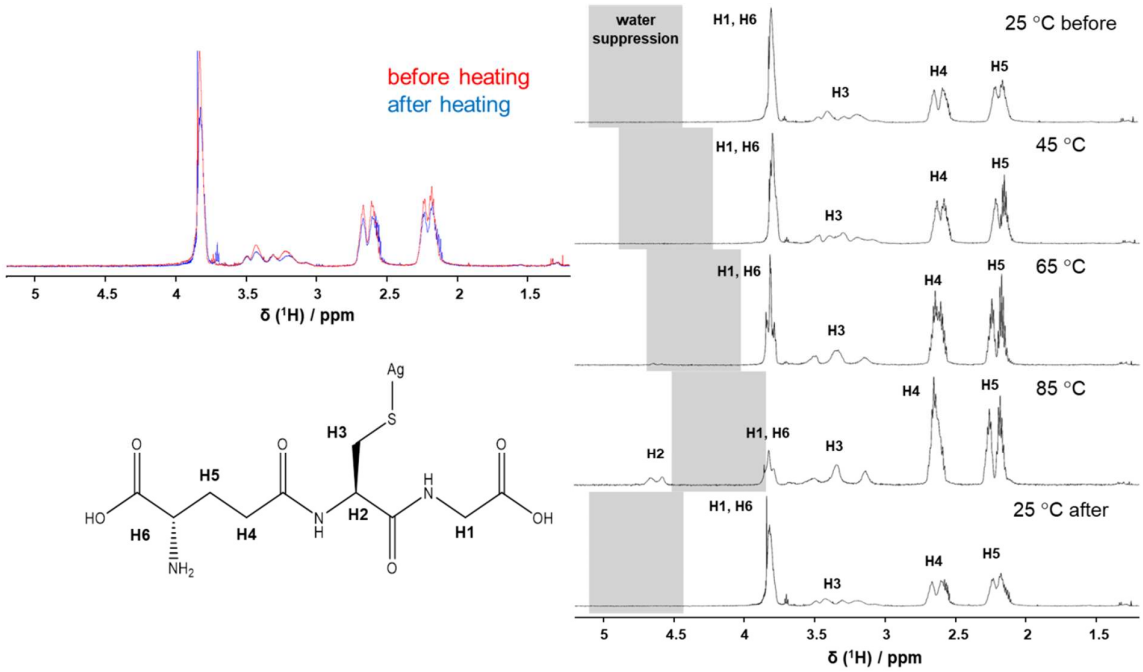

Figure 14: ^{1}H-NMR spectrum of dispersed GSH-coated silver nanoparticles, recorded at variable temperature. Note that the suppression of the water signal (highlighted in grey) and its temperature-dependent shift lead to partially reduced signal intensities (H1, H6) and even to a complete suppression of the signal (H2). The chemical shifts were temperature-corrected according to Nudelman et al.[115]

Finally, the biological effects of the nanoparticles were investigated. The nanoparticles were easily taken up by cells as expected due to their small size. Figure 15 shows their uptake and the intracellular localization.[93, 116, 117] The particles entered the cytoplasm but not the cell nucleus.

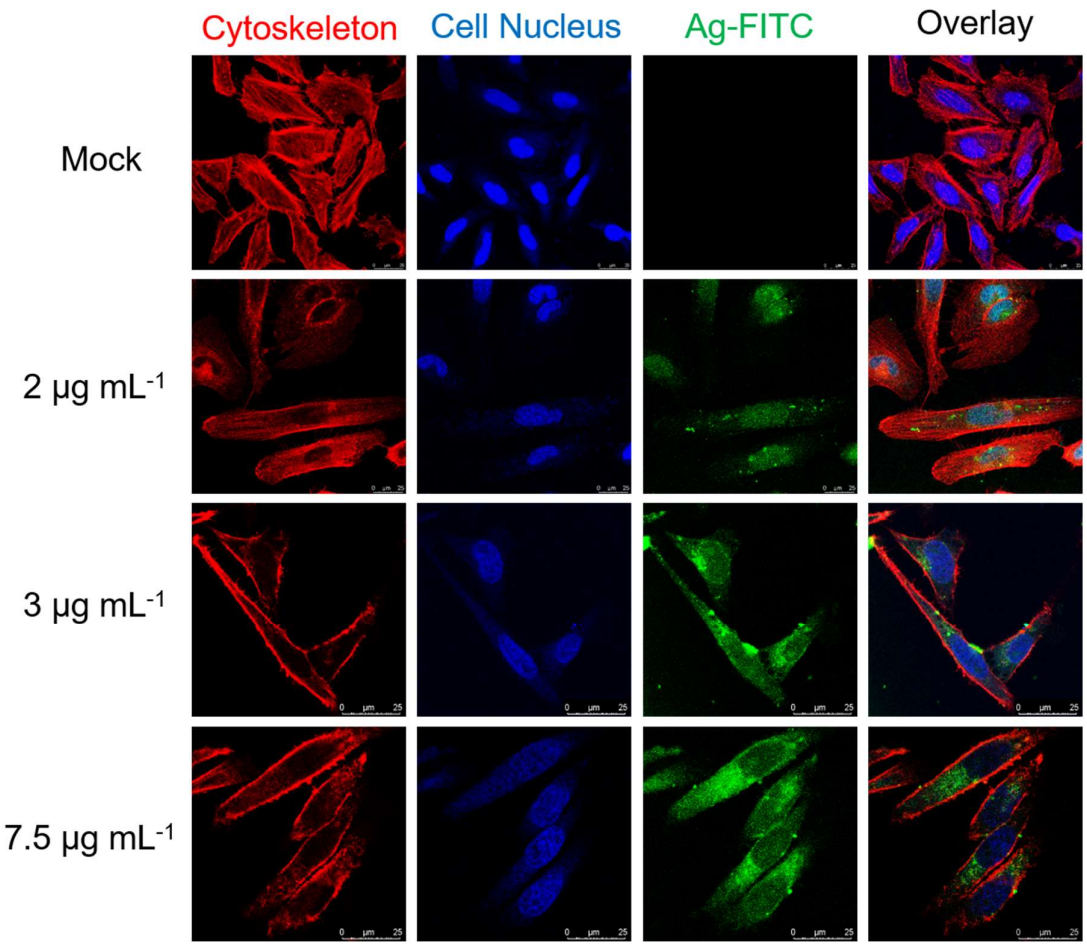

Figure 15: Uptake of GSH-coated fluorescein-labelled silver nanoparticles (green) by HeLa cells after 24 h incubation. The nanoparticles were well taken up by the cells.

The nanoparticles had a comparatively high cytotoxicity where about 50% of the cells were dead at about 15 µg mL^{-1} after 3 h and at about 1 µg mL^{-1} after 24 h (Figure 16). This illustrates the dissolution after uptake by the cells under release of silver ions. This critical concentration is much lower than that observed for larger silver nanoparticles,[42] e.g. 70 nm, where adverse effects did not occur below about 30 µg mL^{-1}.[118] It has been proposed that such an enhanced cytotoxic action of ultrasmall silver nanoparticles can also be used to fight bacteria.[7, 14, 15]

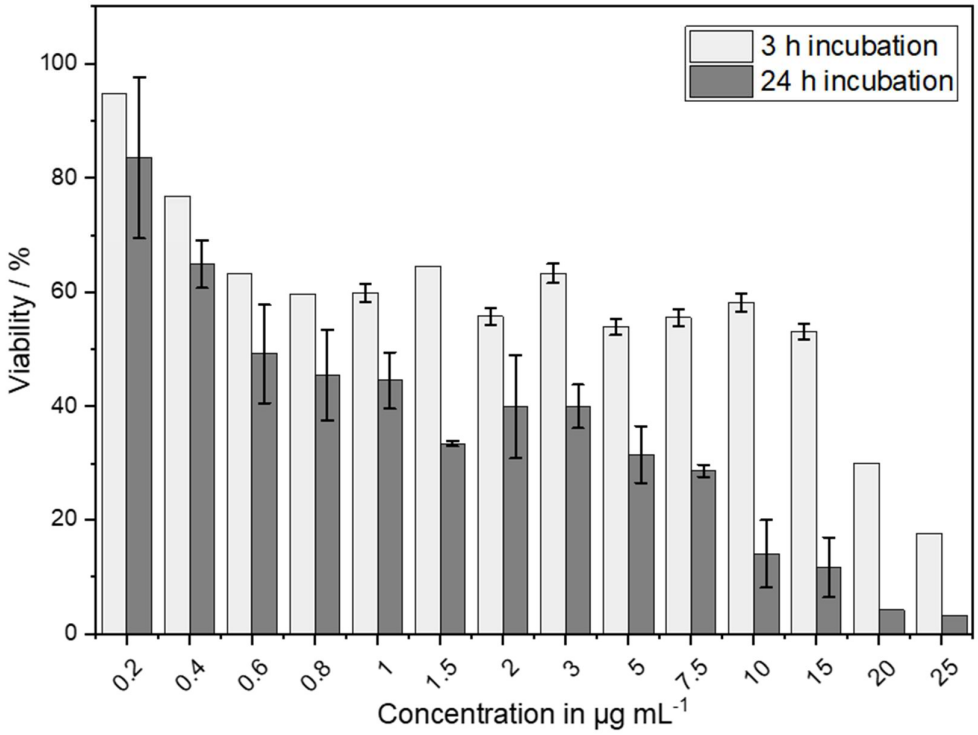

Figure 16: Cytotoxicity of ultrasmall silver nanoparticles on HeLa cells. The particles had an increasingly toxic effect with increasing concentration and time.

Conclusions

Ultrasmall silver nanoparticles, coated with glutathione, can be prepared in considerable amounts (10 mg per synthesis) by a reproducible Brust-Schiffrin synthesis. They have a diameter of the metallic core of about 2 nm (2.4 nm by TEM; 1.6 nm by SAXS), a hydrodynamic diameter of 2 to 2.8 nm (DCS, DOSY), and are well dispersible in water (DCS, DOSY, SAXS). Their internal structure is clearly crystalline with the fcc structure of elemental silver, but surprisingly twinned with crystalline domains of about 0.9 nm in size. As one silver particle consists of about 250 silver atoms, each domain cannot contain more than about 125 silver atoms, and possibly less should each particle contain more than one domain. The surface loading is high (150 to 160 glutathione molecules per nanoparticle) with a ligand footprint of 0.08 nm^2. Thus, we can assume a

stoichiometry of $Ag_{\sim 250}GSH_{\sim 155}$. The interface between the silver atoms and the glutathione molecules can be accessed by XPS. The binding clearly occurs via the thiol group of the central cysteine in glutathione with oxidation to silver(+I) and deprotonation of thiol to thiolate(-). The attached glutathione remains fully intact with all cysteine molecules pointing towards the silver surface as ^{1}H-NMR and ^{13}C-NMR spectroscopy clearly show. By NMR, there are indications of different adsorption sites on the silver surface, but this is close to the limit of the method. NMR at elevated temperature shows that a ligand exchange or release does not occur up to 85 °C in aqueous dispersion. Thus, the silver-glutathione bond is highly stable and not subject to rupture or re-orientation higher temperature. Finally, the particles have a remarkably high cytotoxicity after cellular uptake which is obviously related to their high specific surface area and the enhanced release of toxic silver ions inside the cell.

Supporting Information

High resolution X-ray photoelectron spectra of C 1s (**a**), N 1s (**b**) and O 1s (**c**) obtained for GSH-coated silver nanoparticles.

Acknowledgements

The authors acknowledge financial support by the Deutsche Forschungsgemeinschaft (DFG) in the framework of the Collaborative Research Center SFB 1093: Supramolecular Chemistry on Proteins. We thank Beate Römer and Robin Meya for elemental analyses. Sebastian Leiting (MPI Kohlenforschung, Mülheim) is gratefully acknowledged for XPS measurements. We thank the Imaging Centre Campus Essen (ICCE) for access to the confocal laser scanning microscopes.

Graphical abstract

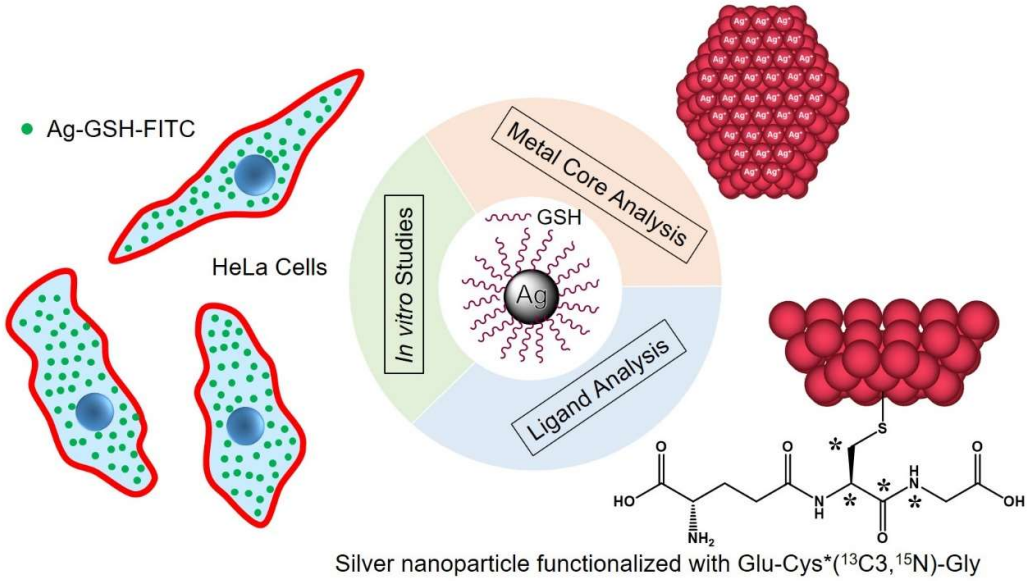

References

1. Turkevich, J.; Stevenson, P. C.; Hilliery, J., A study of the nucleation and growth processes in the synthesis of colloidal gold. *Discuss. Faraday Soc.* **1951,** *11*, 55.
2. Brust, M.; Fink, J.; Bethell, D.; Schiffrin, D. J.; Kiely, C., Synthesis and reactions of functionalised gold nanoparticles. *Chem. Commun.* **1995**, 1655-1656.
3. Brust, M.; Kiely, C. J., Some recent advances in nanostructure preparation from gold and silver particles: a short topical review. *Coll. Surf. A* **2002,** *202*, 175-186.
4. Liz-Marzán, L. M., Gold nanoparticle research before and after the Brust–Schiffrin method. *Chem. Comm.* **2013,** *49* (1), 16-18.
5. Du, X. S.; Jin, R. C., Atomic-precision engineering of metal nanoclusters. *Dalton Trans.* **2020,** *49*, 10701-10707.
6. Zarschler, K.; Rocks, L.; Licciardello, N.; Boselli, L.; Polo, E.; Garcia, K. P.; De Cola, L.; Stephan, H.; Dawson, K. A., Ultrasmall inorganic nanoparticles: State-of-the-art and perspectives for biomedical applications. *Nanomedicine* **2016,** *12*, 1663-1701.
7. Zheng, K. Y.; Yuan, X.; Goswami, N.; Zhang, Q. B.; Xie, J. P., Recent advances in the synthesis, characterization, and biomedical applications of ultrasmall thiolated silver nanoclusters. *RSC Adv.* **2014,** *4*, 60581-60596.
8. Kim, N. H.; Hackett, M. J.; Park, J.; Hyeon, T., Synthesis, characterization, and application of ultrasmall nanoparticles. *Chem. Mater.* **2014,** *26*, 59-71.
9. Leifert, A.; Pan-Bartnek, Y.; Simon, U.; Jahnen-Dechent, W., Molecularly stabilised ultrasmall gold nanoparticles: synthesis, characterization and bioactivity. *Nanoscale* **2013,** *5*, 6224-6242.
10. Meister, A.; Anderson, A. E., Glutathione. *Ann. Rev. Biochem.* **1983,** *52*, 711-760.
11. Guo, C.; Yarger, J. L., Characterizing gold nanoparticles by NMR spectroscopy. *Magn. Reson. Chem.* **2018,** *56*, 1074-1082.
12. Kumar, S.; Bolan, M. D.; Bigioni, T. P., Glutathione-stabilized magic-number silver cluster compounds. *J. Am. Chem. Soc.* **2010,** *132*, 13141-13143.
13. Zan, X. F.; Li, Q. Z.; Pan, Y. T.; Morris, D. J.; Zhang, P.; Li, P.; Yu, H. Z.; Zhu, M. Z., Versatile ligand-exchange method for the synthesis of water-soluble monodisperse AuAg nanoclusters for cancer therapy. *ACS Appl. Nano Mater.* **2018,** *1*, 6773-6781.
14. Jin, J. C.; Wu, X. J.; Xu, J.; Wang, B. B.; Jiang, F. L.; Liu, Y., Ultrasmall silver nanoclusters: Highly efficient antibacterial activity and their mechanisms. *Biomater. Sci.* **2017,** *5*, 247-257.
15. Luo, Z.; Zheng, K.; Xie, J., Engineering ultrasmall water-soluble gold and silver nanoclusters for biomedical applications. *Chem. Comm.* **2014,** *50*, 5143-5155.
16. Shang, L.; Dörlich, R. M.; Trouillet, V.; Bruns, M.; Nienhaus, G. U., Ultrasmall fluorescent silver nanoclusters: protein adsorption and its effects on cellular responses. *Nano Res.* **2012,** *5*, 531-542.
17. Shang, L.; Dong, S. J.; Nienhaus, G. U., Ultra-small fluorescent metal nanoclusters: Synthesis and biological applications. *Nano Today* **2011,** *6*, 401-418.
18. Zhu, L.; Gharib, M.; Becker, C.; Zeng, Y.; Ziefuß, A. R.; Chen, L.; Alkilany, A. M.; Rehbock, C.; Barcikowski, S.; Parak, W. J., et al., Synthesis of fluorescent silver nanoclusters: Introducing bottom-up and top-down approaches to nanochemistry in a single laboratory class. *J. Chem. Educ.* **2020,** *97*, 239-243.
19. Alhilaly, M. J.; Bootharaju, M. S.; Joshi, C. P.; Besong, T. M.; Emwas, A. H.; Juarez-Mosqueda, R.; Kaappa, S.; Malola, S.; Adil, K.; Shkurenko, A., et al., Ag-

67(SPhMe2)(32)(PPh3)(8) (3+): Synthesis, total structure, and optical properties of a large box-shaped silver nanocluster. *J. Am. Chem. Soc.* **2016,** *138*, 14727-14732.
20. Kästner, C.; Saloga, P. E. J.; Thünemann, A. F., Kinetic monitoring of glutathione-induced silver nanoparticle disintegration. *Nanoscale* **2018,** *10*, 11485-11490.
21. Saloga, P. E. J.; Kastner, C.; Thunemann, A. F., High-speed but not magic: Microwave-assisted synthesis of ultra-small silver nanoparticles. *Langmuir* **2018,** *34*, 147-153.
22. Chakraborty, I.; Govindarajan, A.; Erusappan, J.; Ghosh, A.; Pradeep, T.; Yoon, B.; Whetten, R. L.; Landman, U., The superstable 25 kDa monolayer protected silver nanoparticle: Measurements and interpretation as an icosahedral Ag-152(SCH2CH2Ph)(60) cluster. *Nano Lett.* **2012,** *12*, 5861-5866.
23. Desireddy, A.; Conn, B. E.; Guo, J. S.; Yoon, B.; Barnett, R. N.; Monahan, B. M.; Kirschbaum, K.; Griffith, W. P.; Whetten, R. L.; Landman, U., et al., Ultrastable silver nanoparticles. *Nature* **2013,** *501* (7467), 399-402.
24. Lopez, P.; Lara, H. H.; Mullins, S. M.; Black, D. M.; Ramsower, H. M.; Alvarez, M. M.; Williams, T. L.; Lopez-Lozano, X.; Weissker, H. C.; Garcia, A. P., et al., Tetrahedral (T) closed-shell cluster of 29 silver atoms & 12 lipoate ligands, Ag-29(R-alpha-LA)(12) ((3-)): Antibacterial and antifungal activity. *ACS Appl. Nano Mater.* **2018,** *1*, 1595-1602.
25. Weissker, H. C.; Whetten, R. L.; Lopez-Lozano, X., Optical response of quantum-sized Ag and Au clusters - cage vs. compact structures and the remarkable insensitivity to compression. *Phys. Chem. Chem. Phys.* **2014,** *16*, 12495-12502.
26. Cathcart, N.; Mistry, P.; Makra, C.; Pietrobon, B.; Coombs, N.; Jelokhani-Niaraki, M.; Kitaev, V., Chiral thiol-stabilized silver nanoclusters with well-resolved optical transitions synthesized by a facile etching procedure in aqueous solutions. *Langmuir* **2009,** *25*, 5840-5846.
27. Le Guével, X.; Spies, C.; Daum, N.; Jung, G.; Schneider, M., Highly fluorescent silver nanoclusters stabilized by glutathione: a promising fluorescent label for bioimaging. *Nano Res.* **2012,** *5*, 379-387.
28. Park, J.; Kwon, S. G.; Jun, S. W.; Kim, B. H.; Hyeon, T., Large-scale synthesis of ultra-small-sized silver nanoparticles. *ChemPhysChem* **2012,** *13*, 2540-2543.
29. Cathcart, N.; Kitaev, V., Silver nanoclusters: single-stage scaleable synthesis of monodisperse species and their chirooptical properties. *J. Phys. Chem. C* **2010,** *114*, 16010-16017.
30. Xu, H.; Suslick, K. S., Water-soluble fluorescent silver nanoclusters. *Adv. Mater.* **2010,** *22*, 1078-1082.
31. Guisbiers, G.; Mendoza-Cruz, R.; Bazan-Diaz, L.; Velazquez-Salazar, J. J.; Mendoza-Perez, R.; Robledo-Torres, J. A.; Rodriguez-Lopez, J. L.; Montejano-Carrizales, J. M.; Whetten, R. L.; Jose-Yacaman, M., Electrum, the gold–silver alloy, from the bulk scale to the nanoscale: synthesis, properties, and segregation rules. *ACS Nano* **2016,** *10*, 188-198.
32. Ristig, S.; Kozlova, D.; Meyer-Zaika, W.; Epple, M., An easy synthesis of autofluorescent alloyed silver-gold nanoparticles. *J. Mater. Chem. B* **2014,** *2*, 7887-7895.
33. Zhou, T. Y.; Lin, L. P.; Rong, M. C.; Jiang, Y. Q.; Chen, X., Silver-gold alloy nanoclusters as a fluorescence-enhanced probe for aluminum ion sensing. *Anal. Chem.* **2013,** *85*, 9839-9844.
34. Dong, X. Y.; Gao, Z. W.; Yang, K. F.; Zhang, W. Q.; Xu, L. W., Nanosilver as a new generation of silver catalysts in organic transformations for efficient synthesis of fine chemicals. *Catal. Sci. Technol.* **2015,** *5*, 2554-2574.
35. Gao, Y.; Jiang, P.; Song, L.; Liu, L.; Yan, X.; Zhou, Z.; Liu, D.; Wang, J.; Yuan, H.; Zhang, Z., et al., Growth mechanism of silver nanowires synthesized by polyvinylpyrrolidone-assisted polyol reduction. *J. Phys. D: Appl. Phys.* **2005,** *38*, 1061-1067.

36. Choi, H.; Ko, S. J.; Choi, Y.; Joo, P.; Kim, T.; Lee, B. R.; Jung, J. W.; Choi, H. J.; Cha, M.; Jeong, J. R., et al., Versatile surface plasmon resonance of carbon-dot-supported silver nanoparticles in polymer optoelectronic devices. *Nat. Photonics* **2013,** *7*, 732-738.
37. Hu, M. S.; Chen, H. L.; Shen, C. H.; Hong, L. S.; Huang, B. R.; Chen, K. H.; Chen, L. C., Photosensitive gold-nanoparticle-embedded dielectric nanowires. *Nat. Mater.* **2006,** *5*, 102-106.
38. Kauranen, M.; Zayats, A. V., Nonlinear plasmonics. *Nat. Photonics* **2012,** *6*, 737-748.
39. Chen, X.; Schluesener, H. J., Nanosilver: A nanoproduct in medical application. *Toxicol. Lett.* **2008,** *176*, 1-12.
40. Howes, P. D.; Chandrawati, R.; Stevens, M. M., Colloidal nanoparticles as advanced biological sensors. *Science* **2014,** *346*, 1247390.
41. Linic, S.; Christopher, P.; Ingram, D. B., Plasmonic-metal nanostructures for efficient conversion of solar to chemical energy. *Nat. Mater.* **2011,** *10*, 911-921.
42. Chernousova, S.; Epple, M., Silver as antibacterial agent: Ion, nanoparticle, metal. *Angew. Chem. Int. Ed.* **2013,** *52*, 1636-1653.
43. Huo, S.; Jin, S.; Ma, X.; Xue, X.; Yang, K.; Kumar, A.; Wang, P. C.; Zhang, J.; Hu, Z.; Liang, X. J., Ultrasmall gold nanoparticles as carriers for nucleus-based gene therapy due to size-dependent nuclear entry. *ACS Nano* **2014,** *8*, 5852-5862.
44. Sokolova, V.; Nzou, G.; van der Meer, S. B.; Ruks, T.; Heggen, M.; Loza, K.; Hagemann, N.; Murke, F.; Giebel, B.; Hermann, D. M., et al., Ultrasmall gold nanoparticles (2 nm) can penetrate and enter cell nuclei in an in-vitro brain spheroid model. *Acta Biomater.* **2020,** *111*, 349-362.
45. Harush-Frenkel, O.; Debotton, N.; Benita, S.; Altschuler, Y., Targeting of nanoparticles to the clathrin-mediated endocytic pathway. *Biochem. Biophys. Res. Commun.* **2007,** *353*, 26-32.
46. Cha, K.; Hong, H. W.; Choi, Y. G.; Lee, M. J.; Park, J. H.; Chae, H. K.; Ryu, G.; Myung, H., Comparison of acute responses of mice livers to short-term exposure to nano-sized or micro-sized silver particles. *Biotechnol. Lett.* **2008,** *30*, 1893-1899.
47. Chung, Y. C.; Chen, I. H.; Chen, C. J., The surface modification of silver nanoparticles by phosphoryl disulfides for improved biocompatibility and intracellular uptake. *Biomaterials* **2008,** *29*, 1807-1816.
48. Kastl, L.; Sasse, D.; Wulf, V.; Hartmann, R.; Mircheski, J.; Ranke, C.; Carregal-Romero, S.; Martínez-López, J. A.; Fernández-Chacón, R.; Parak, W. J., et al., Multiple internalization pathways of polyelectrolyte multilayer capsules into mammalian cells. *ACS Nano* **2013,** *7*, 6605-6618.
49. Shang, L.; Nienhaus, K.; Jiang, X.; Yang, L.; Landfester, K.; Mailänder, V.; Simmet, T.; Nienhaus, G. U., Nanoparticle interactions with live cells: Quantitative fluorescence microscopy of nanoparticle size effects. *Beilstein J. Nanotechnol.* **2014,** *5*, 2388-2397.
50. Kuhn, D. A.; Vanhecke, D.; Michen, B.; Blank, F.; Gehr, P.; Petri-Fink, A.; Rothen-Rutishauser, B., Different endocytotic uptake mechanisms for nanoparticles in epithelial cells and macrophages. *Beilstein J. Nanotechnol.* **2014,** *5*, 1625-1636.
51. Helmlinger, J.; Sengstock, C.; Gross-Heitfeld, C.; Mayer, C.; Schildhauer, T. A.; Köller, M.; Epple, M., Silver nanoparticles with different size and shape: equal cytotoxicity, but different antibacterial effects. *RSC Adv.* **2016,** *6*, 18490-18501.
52. Sotiriou, G. A.; Pratsinis, S. E., Engineering nanosilver as an antibacterial, biosensor and bioimaging material. *Curr. Opinion Chem. Eng.* **2011,** *1*, 3-10.
53. Pakiari, A. H.; Jamshidi, Z., Nature and strength of M-S bonds (M = Au, Ag, and Cu) in binary alloy gold clusters. *J. Phys. Chem. A* **2010,** *114*, 9212-9221.

54. Juarez-Mosqueda, R.; Kaappa, S.; Malola, S.; Hakkinen, H., Analysis of the electronic structure of non-spherical ligand-protected metal nanoclusters: the case of a box-like Ag-67. *J. Phys. Chem. C* **2017,** *121*, 10698-10705.
55. Kang, X.; Li, Y. W.; Zhu, M. Z.; Jin, R. C., Atomically precise alloy nanoclusters: syntheses, structures, and properties. *Chem. Soc. Rev.* **2020,** *49*, 6443-6514.
56. Masters, J. R., HeLa cells 50 years on: the good, the bad and the ugly. *Nat. Rev. Cancer* **2002,** *2*, 315-319.
57. Thust, A.; Barthel, J.; Tillmann, K., FEI Titan 80-300 TEM. *J. Large-scale Res. Fac.* **2016,** *2*, A41.
58. Akoka, S.; Barantin, L.; Trierweiler, M., Concentration measurement by proton NMR using the ERETIC method. *Anal. Chem.* **1999,** *71*, 2554-2557.
59. Altieri, A. S.; Hinton, D. P.; Byrd, R. A., Association of biomolecular systems via pulsed-field gradient NMR self-diffusion measurements. *J. Am. Chem. Soc.* **1995,** *117*, 7566-7567.
60. Stejskal, E. O.; Tanner, J. E., Spin diffusion measurements: Spin echoes in the presence of a time-dependent field gradient. *J. Chem. Phys.* **1965,** *42*, 288.
61. Millero, F. J.; Dexter, R.; Hoff, E., Density and viscosity of deuterium oxide solutions from 5-70 °C. *J. Chem. Eng. Data* **1971,** *16*, 85-87.
62. Powder Diffraction File (PDF) 00-004-0783 (Ag). *International Centre for Diffraction Data (ICDD)*.
63. Powder Diffraction File (PDF) 00-034-0427 (LaB_6). *International Centre for Diffraction Data (ICDD)*.
64. Scherrer, P., Bestimmung der Größe und der inneren Struktur von Kolloidteilchen mittels Röntgenstrahlen. *Nachr. Ges. Wiss. Göttingen* **1918,** *2*, 98-100.
65. Klug, H. P.; Alexander, L. E., *X-ray diffraction procedures for polycrystalline and amorphous materials*. Wiley-Interscience: New York, 1974.
66. Semenyuk, A. V.; Svergun, D. I., GNOM– a program package for small-angle scattering data processing. *J. Appl. Crystallogr.* **1991,** *24*, 537-540.
67. Lindner, P.; Zemb, T., *Neutron, X-ray and light scattering: introduction to an investigative tool for colloidal and polymeric systems*. Amsterdam, 1991.
68. Craievich, A. F., Small-angle X-ray scattering by nanostructured materials. In *Handbook of Sol-Gel Science and Technology*, L., K.; Aparicio, M.; Jitianu, A., Eds. Springer: 2016.
69. Grant, T. D.; Luft, J. R.; Carter, L. G.; Matsui, T.; Weiss, T. M.; Martel, A.; Snell, E. H., The accurate assessment of small-angle X-ray scattering data. *Acta Crystallogr. D Biol. Crystallogr.* **2015,** *71* (Pt 1), 45-56.
70. Fissan, H.; Ristig, S.; Kaminski, H.; Asbach, C.; Epple, M., Comparison of different characterization methods for nanoparticle dispersions before and after aerosolization. *Anal. Meth.* **2014,** *6*, 7324-7334.
71. Langer, J.; Novikov, S. M.; Liz-Marzán, L. M., Sensing using plasmonic nanostructures and nanoparticles. *Nanotechnology* **2015,** *26*, 322001.
72. Yu, R.; Liz-Marzán, L. M.; García de Abajo, F. J., Universal analytical modeling of plasmonic nanoparticles. *Chem. Soc. Rev.* **2017,** *46*, 6710-6724.
73. Ristig, S.; Prymak, O.; Loza, K.; Gocyla, M.; Meyer-Zaika, W.; Heggen, M.; Raabe, D.; Epple, M., Nanostructure of wet-chemically prepared, polymer-stabilized silver–gold nanoalloys (6 nm) over the entire composition range. *J. Mater. Chem. B* **2015,** *3*, 4654-4662.
74. Prymak, O.; Grasmik, V.; Loza, K.; Heggen, M.; Epple, M., Temperature-induced stress relaxation in alloyed silver–gold nanoparticles (7–8 nm) by in situ x-ray powder diffraction. *Cryst. Growth Des.* **2020,** *20*, 107-115.

75. Qi, W. H.; Wang, M. P., Size and shape dependent lattice parameters of metallic nanoparticles. *J. Nanoparticle Res.* **2005,** *7*, 51-57.
76. Ruks, T.; Loza, K.; Heggen, M.; Prymak, O.; Sehnem, A. L.; Oliveira, C. L. P.; Bayer, P.; Beuck, C.; Epple, M., Peptide-conjugated ultrasmall gold nanoparticles (2 nm) for selective protein targeting. *ACS Appl. Bio Mater.* **2021,** *4*, 945-965.
77. Banerjee, S.; Liu, C. H.; Lee, J. D.; Kovyakh, A.; Grasmik, V.; Prymak, O.; Koenigsmann, C.; Liu, H.; Wang, L.; Abeykoon, A. M. M., et al., Improved models for metallic nanoparticle cores from atomic pair distribution function (PDF) analysis. *J. Phys. Chem. C* **2018,** *122*, 29498-29506.
78. Yan, J. Z.; Malola, S.; Hu, C. Y.; Peng, J.; Dittrich, B.; Teo, B. K.; Hakkinen, H.; Zheng, L. S.; Zheng, N. F., Co-crystallization of atomically precise metal nanoparticles driven by magic atomic and electronic shells. *Nat. Commun.* **2018,** *9*, 3357.
79. Kenzler, S.; Schrenk, C.; Frojd, A. R.; Hakkinen, H.; Clayborne, A. Z.; Schnepf, A., $Au_{70}S_{20}(PPh_3)_{12}$: an intermediate sized metalloid gold cluster stabilized by the Au_4S_4 ring motif and Au-PPh_3 groups. *Chem. Comm.* **2018,** *54*, 248-251.
80. Azubel, M.; Koh, A. L.; Koyasu, K.; Tsukuda, T.; Kornberg, R. D., Structure determination of a water-soluble 144-gold atom particle at atomic resolution by aberration-corrected electron microscopy. *ACS Nano* **2017,** *11*, 11866-11871.
81. Jensen, K. M. O.; Juhas, P.; Tofanelli, M. A.; Heinecke, C. L.; Vaughan, G.; Ackerson, C. J.; Billinge, S. J. L., Polymorphism in magic-sized Au144(SR)60 clusters. *Nat. Commun.* **2016,** *7*, 11859.
82. Chen, Y.; Zeng, C.; Liu, C.; Kirschbaum, K.; Gayathri, C.; Gil, R. R.; Rosi, N. L.; Jin, R., Crystal structure of barrel-shaped chiral Au130(p-MBT)50 nanocluster. *J. Am. Chem. Soc.* **2015,** *137*, 10076-10079.
83. Jin, R. C.; Nobusada, K., Doping and alloying in atomically precise gold nanoparticles. *Nano Res.* **2014,** *7*, 285-300.
84. Lu, Y.; Chen, W., Sub-nanometre sized metal clusters: from synthetic challenges to the unique property discoveries. *Chem. Soc. Rev.* **2012,** *41*, 3594-3623.
85. Schnoeckel, H.; Schnepf, A.; Whetten, R. L.; Schenk, C.; Henke, P., A chemical view of the giant Au-102(SR)(44) (SR = p-mercaptobenzoic acid) cluster: Metalloid aluminum and gallium clusters as path making examples of this novel type open our eyes for structure and bonding of metalloid Au-n(SR)(m) (n > m) clusters. *Z. Anorg. Allg. Chem.* **2011,** *637*, 15-23.
86. Parker, J. F.; Fields-Zinna, C. A.; Murray, R. W., The story of a monodisperse gold nanoparticle: $Au_{25}L_{18}$. *Acc. Chem. Res.* **2010,** *43*, 1289-1296.
87. Jin, R., Quantum sized, thiolate-protected gold nanoclusters. *Nanoscale* **2010,** *2*, 343-362.
88. Fetzer, F.; Maier, A.; Hodas, M.; Geladari, O.; Braun, K.; Meixner, A. J.; Schreiber, F.; Schnepf, A.; Scheele, M., Structural order enhances charge carrier transport in self-assembled Au-nanoclusters. *Nat. Commun.* **2020,** *11*, 6188.
89. Garcia, P. R. A. F.; Prymak, O.; Grasmik, V.; Pappert, K.; Wlysses, W.; Otubo, L.; Epple, M.; Oliveira, C. L. P., An in situ SAXS investigation of the formation of silver nanoparticles and bimetallic silver–gold nanoparticles in controlled wet-chemical reduction synthesis. *Nanoscale Adv.* **2019,** *2*, 225-238.
90. Garcia, P. R. A. F.; Loza, K.; Daumann, S.; Grasmik, V.; Pappert, K.; Rostek, A.; Helmlinger, J.; Prymak, O.; Heggen, M.; Epple, M., et al., Combining small-angle x-ray scattering and x-ray powder diffraction to investigate size, shape and crystallinity of silver, gold and alloyed silver-gold nanoparticles. *Braz. J. Phys.* **2019,** *49*, 183-190.

91. Nützenadel, C.; Züttel, A.; Chartouni, D.; Schmid, G.; Schlapbach, L., Critical size and surface effect of the hydrogen interaction of palladium clusters. *Eur. Phys. J. D* **2000,** *8*, 245-250.
92. van der Meer, S. B.; Seiler, T.; Buchmann, C.; Partalidou, G.; Boden, S.; Loza, K.; Heggen, M.; Linders, J.; Prymak, O.; Oliveira, C. L. P., et al., Controlling the surface functionalization of ultrasmall gold nanoparticles by sequence-defined macromolecules. *Chem. Eur. J.* **2021,** *27*, 1451-1464.
93. van der Meer, S. B.; Loza, K.; Wey, K.; Heggen, M.; Beuck, C.; Bayer, P.; Epple, M., Click chemistry on the surface of ultrasmall gold nanoparticles (2 nm) for covalent ligand attachment followed by NMR spectroscopy. *Langmuir* **2019,** *35*, 7191-7204.
94. Ruks, T.; Beuck, C.; Schaller, T.; Niemeyer, F.; Zähres, M.; Loza, K.; Heggen, M.; Hagemann, U.; Mayer, C.; Bayer, P., et al., Solution NMR spectroscopy with isotope-labelled cysteine (^{13}C, ^{15}N) reveals the surface structure of L-cysteine-coated ultrasmall gold nanoparticles (1.8 nm). *Langmuir* **2019,** *35*, 767-778.
95. Marbella, L. E.; Millstone, J. E., NMR techniques for noble metal nanoparticles. *Chem. Mater.* **2015,** *27*, 2721-2739.
96. Schuetze, B.; Mayer, C.; Loza, K.; Gocyla, M.; Heggen, M.; Epple, M., Conjugation of thiol-terminated molecules to ultrasmall 2 nm-gold nanoparticles leads to remarkably complex 1H-NMR spectra. *J. Mater. Chem. B* **2016,** *4*, 2179-2189.
97. Salassa, G.; Burgi, T., NMR spectroscopy: a potent tool for studying monolayer-protected metal nanoclusters. *Nanoscale Horiz.* **2018,** *3*, 8.
98. Ebbesen, M. F.; Gerke, C.; Hartwig, P.; Hartmann, L., Biodegradable poly(amidoamine)s with uniform degradation fragments via sequence-controlled macromonomers. *Polym. Chem.* **2016,** *7*, 7086-7093.
99. Heid, C.; Sowislok, A.; Schaller, T.; Niemeyer, F.; Klärner, F. G.; Schrader, T., Molecular tweezers with additional recognition sites. *Chem. Eur. J.* **2018,** *24*, 11332-11343.
100. van der Meer, S. B.; Hadrovic, I.; Meiners, A.; Loza, K.; Heggen, M.; Knauer, S. K.; Bayer, P.; Schrader, T.; Beuck, C.; Epple, M., New tools to probe the protein surface: ultrasmall gold nanoparticles carry amino acid binders. *J. Phys. Chem. B* **2021,** *125*, 115-127.
101. Ruks, T.; Loza, K.; Heggen, M.; Ottmann, C.; Bayer, P.; Beuck, C.; Epple, M., Targeting the surface of the protein 14-3-3 by ultrasmall gold nanoparticles (1.5 nm), carrying the specific peptide CRaf. *ChemBioChem* **2021,** *22*, 1456-1463.
102. Häkkinen, H.; Walter, M.; Grönbeck, H., Divide and protect: Capping gold nanoclusters with molecular gold−thiolate rings. *J. Phys. Chem. B* **2006,** *110*, 9927-9931.
103. Häkkinen, H., The gold–sulfur interface at the nanoscale. *Nat. Chem.* **2012,** *4*, 443-455.
104. Juarez-Mosqueda, R.; Malola, S.; Hakkinen, H., Stability, electronic structure, and optical properties of protected gold-doped silver Ag(29-x)Au(x) (x=0-5) nanoclusters. *Phys. Chem. Chem. Phys.* **2017,** *19*, 13868-13874.
105. Ferraria, A. M.; Carapeto, A. P.; do Rego, A. M. B., X-ray photoelectron spectroscopy: Silver salts revisited. *Vacuum* **2012,** *86*, 1988-1991.
106. Kaushik, V. K., XPS core level spectra and Auger parameters for some silver compounds. *J. Electron Spectrosc. Relat. Phenom.* **1991,** *56*, 273-277.
107. Bensebaa, F.; Yu, Z.; Deslandes, Y.; Kruus, E.; Ellis, T. H., XPS study of metal-sulfur bonds in metal-alkanethiolate materials. *Surf. Sci.* **1998,** *405* (1), L472-L476.
108. Porcaro, F.; Carlini, L.; Ugolini, A.; Visaggio, D.; Visca, P.; Fratoddi, I.; Venditti, I.; Meneghini, C.; Simonelli, L.; Marini, C., et al., Synthesis and structural characterization of silver nanoparticles stabilized with 3-mercapto-1-propansulfonate and 1-thioglucose mixed thiols for antibacterial applications. *Materials* **2016,** *9*, 1028.

109. Zhang, S.; Leem, G.; Lee, T. R., Monolayer-protected gold nanoparticles prepared using long-chain alkanethioacetates. *Langmuir* **2009,** *25*, 13855-13860.
110. Castner, D. G.; Hinds, K.; Grainger, D. W., X-ray photoelectron spectroscopy sulfur 2p study of organic thiol and disulfide binding interactions with gold surfaces. *Langmuir* **1996,** *12* (21), 5083-5086.
111. Calborean, A.; Martin, F.; Marconi, D.; Turcu, R.; Kacso, I. E.; Buimaga-Iarinca, L.; Graur, F.; Turcu, I., Adsorption mechanisms of L-glutathione on Au and controlled nano-patterning through Dip Pen Nanolithography. *Mater. Sci. Eng. C-Mater. Biol. Appl.* **2015,** *57*, 171-180.
112. Sayevich, V.; Guhrenz, C.; Dzhagan, V. M.; Sin, M.; Werheid, M.; Cai, B.; Borchardt, L.; Widmer, J.; Zahn, D. R. T.; Brunner, E., et al., Hybrid N-butylamine-based ligands for switching the colloidal solubility and regimentation of inorganic-capped nanocrystals. *ACS Nano* **2017,** *11*, 1559-1571.
113. Volkert, A. A.; Subramaniam, V.; Ivanov, M. R.; Goodman, A. M.; Haes, A. J., Salt-mediated self-assembly of thioctic acid on gold nanoparticles. *ACS Nano* **2011,** *5*, 4570-4580.
114. Bootharaju, M. S.; Burlakov, V. M.; Besong, T. M. D.; Joshi, C. P.; AbdulHalim, L. G.; Black, D. M.; Whetten, R. L.; Goriely, A.; Bakr, O. M., Reversible size control of silver nanoclusters via ligand-exchange. *Chem. Mater.* **2015,** *27*, 4289-4297.
115. Gottlieb, H. E.; Kotlyar, V.; Nudelman, A., NMR chemical shifts of common laboratory solvents as trace impurities. *J. Org. Chem.* **1997,** *62*, 7512-7515.
116. Dahmani, F. Z.; Zhong, D. N.; Qi, Y. C.; Dahmani, A. E.; Xie, T. T.; Zhou, B.; Li, W. L.; Yao, K.; Li, L.; Zhou, M., A size-tunable and multi-responsive nanoplatform for deep tumor penetration and targeted combinatorial radio-/chemotherapy. *J. Mater. Chem. B* **2019,** *7*, 4484-4498.
117. Zhang, X.; Shastry, S.; Bradforth, S. E.; Nadeau, J. L., Nuclear uptake of ultrasmall gold-doxorubicin conjugates imaged by fluorescence lifetime imaging microscopy (FLIM) and electron microscopy. *Nanoscale* **2015,** *7*, 240-251.
118. Ahlberg, S.; Antonopulos, A.; Diendorf, J.; Dringen, R.; Epple, M.; Flöck, R.; Goedecke, W.; Graf, C.; Haberl, N.; Helmlinger, J., et al., PVP-coated, negatively charged silver nanoparticles: A multi-center study of their physicochemical characteristics, cell culture and in vivo experiments. *Beilstein J. Nanotechnol.* **2014,** *5*, 1944-1965.